



**Michigan
Technological
University**

Michigan Technological University
Digital Commons @ Michigan Tech

Dissertations, Master's Theses and Master's Reports

2017

MICROSTRUCTURAL EVOLUTION AND MECHANICAL PROPERTIES OF Zn-Ti ALLOYS FOR BIODEGRADABLE STENT APPLICATIONS

Zhiyong Yin
Michigan Technological University, zhyin@mtu.edu

Copyright 2017 Zhiyong Yin

Recommended Citation

Yin, Zhiyong, "MICROSTRUCTURAL EVOLUTION AND MECHANICAL PROPERTIES OF Zn-Ti ALLOYS FOR BIODEGRADABLE STENT APPLICATIONS", Open Access Master's Thesis, Michigan Technological University, 2017.
<https://digitalcommons.mtu.edu/etdr/553>

Follow this and additional works at: <https://digitalcommons.mtu.edu/etdr>



Part of the [Metallurgy Commons](#)

MICROSTRUCTURAL EVOLUTION AND MECHANICAL PROPERTIES OF Zn-Ti
ALLOYS FOR BIODEGRADABLE STENT APPLICATIONS

By
Zhiyong Yin

A THESIS

Submitted in partial fulfillment of the requirements for the degree of

MASTER OF SCIENCE

In Materials Science and Engineering

MICHIGAN TECHNOLOGICAL UNIVERSITY

2017

© 2017 Zhiyong Yin

This thesis has been approved in partial fulfillment of the requirements for the Degree of MASTER OF SCIENCE in Materials Science and Engineering.

Department of Materials Science and Engineering

Thesis Advisor: *Jaroslav Drelich, Ph.D*

Committee Member: *Jeremy Goldman, Ph.D*

Committee Member: *Daniel Seguin, Ph.D*

Department Chair: *Stephen Kampe, Ph.D*

Table of Contents

List of figures.....	v
List of tables.....	vii
Acknowledgements.....	viii
Abstract.....	ix
1 Introduction.....	1
2 Background and Literature Review	5
2.1 Criteria for bioabsorbable stents.....	5
2.2 Biodegradable iron and magnesium materials for stent application	6
2.3 Zinc-based alloys for biodegradable stents	11
2.4 Novel Zn-Ti Alloys for medical application	16
3 Goals and Hypotheses.....	19
4 Experimental Methods and Materials	23
4.1 Materials Preparation	23
4.1.1 Materials	23
4.1.2 Vacuum Induction Melting.....	23
4.1.3 Hot Extrusion.....	25
4.2 Elemental Analysis.....	26
4.3 Microstructural Analysis	27
4.4 X-ray Diffraction (XRD).....	27
4.5 Mechanical Testing	27
4.5.1 Microhardness Measurement.....	27
4.5.2 Tensile Testing.....	28
5 Results and Discussion	29
5.1 Microstructural Characterization.....	29
5.1.1 As-cast Alloys.....	29
5.1.2 Hot-extruded Alloys.....	39
5.2 Microhardness	44
5.2.1 As-cast Alloys.....	44
5.2.2 Hot-extruded Alloys.....	47
5.3 Mechanical Properties	49

5.3.1	As-cast Alloys	49
5.3.2	Hot-extruded Alloys.....	53
5.4	Fractography.....	59
6	Conclusions.....	64
7	Reference List	66
	Appendix A . Copyright documentation.....	73

List of figures

Figure 2.1. Optical micrographs for high purity (HP) and commercial purity (CP) zinc wires.....	17
Figure 3.1. Zn-Ti binary phase diagram: a) 89-100 at% Zn [87], b) Temperature from 417 to 421°C, c) Ti content from 0 to 0.2 at% (estimate based on Ref. [87, 88]).	20
Figure 4.1. Vacuum induction melting furnace.	23
Figure 4.2. Zn-Ti alloy ingot.....	24
Figure 4.3. System setup used in the hot extrusion process.....	25
Figure 4.4. The extrusion die configuration.....	26
Figure 4.5. Samples of Zn-Ti alloy rod: a) before and b) after hot extrusion.....	26
Figure 5.1. Optical micrograph of as-cast Zn-0.01 wt% Ti: a) 25x, b) 100x.	30
Figure 5.2. X-ray diffraction patterns of as-cast Zn-0.01 wt% Ti alloy.	31
Figure 5.3. Optical micrograph of as-cast Zn-0.1 wt% Ti: a) 25x, b) 100x, c) 500x.	32
Figure 5.4. SEM micrograph of as-cast Zn-0.1 wt% Ti: a) 200x, b) 1000x.	33
Figure 5.5. Optical micrograph of as-cast Zn-0.3 wt% Ti: a) 200x, b) 500x.	34
Figure 5.6. EDS point scan of intermetallic phase of as-cast Zn-0.3 wt% Ti alloy.....	34
Figure 5.7. SEM micrograph of as-cast Zn-0.3 wt% Ti.....	34
Figure 5.8. X-ray diffraction patterns of as-cast Zn-0.3 wt% Ti alloy.	35
Figure 5.9. Optical micrograph of as-cast Zn-0.5 wt% Ti: a) 200x, b) 500x.	36
Figure 5.10. SEM micrograph of as-cast Zn-0.5 wt% Ti: a) 200x, b) 500x.	36
Figure 5.11. Optical micrograph of as-cast Zn-1 wt% Ti: a) 200x, b) 500x.	37
Figure 5.12. EDS point scans of as-cast Zn-1 wt% Ti alloy: a) EDS spectrum of point 1, b) EDS spectrum of point 2.	37
Figure 5.13. Optical micrograph of as-cast Zn-2.5 wt% Ti: a) 200x, b) 500x.	38
Figure 5.14. X-ray diffraction patterns of as-cast Zn-2.5 wt% Ti alloy.	39

Figure 5.15. Optical micrograph of as-extruded Zn-0.01 wt% Ti.	40
Figure 5.16. SEM micrograph of as-extruded Zn-0.01 wt% Ti: a) 1000x, b) 2000x.	40
Figure 5.17. X-ray diffraction patterns of as-extruded Zn-0.01 wt% Ti alloy.....	41
Figure 5.18. Optical micrograph of as-extruded Zn-0.1 wt% Ti: a) 50x, b) 200x, and c) 500x.....	42
Figure 5.19. SEM micrograph of as-extruded Zn-0.1 wt% Ti: a) 1000x, b) 2000x.	42
Figure 5.20. Optical micrograph of as-extruded Zn-0.3 wt% Ti: a) 200x, b) 500x.....	43
Figure 5.21. SEM micrograph of as-extruded Zn-0.3 wt% Ti: a) 500x, b) 1000x.	44
Figure 5.22. X-ray diffraction patterns of as-extruded Zn-0.3 wt% Ti alloy.....	44
Figure 5.23. The average hardness for the as-cast Zn-Ti alloys.	46
Figure 5.24. The average hardness for the as-extruded Zn-Ti alloys.	49
Figure 5.25. The average ultimate tensile strength for the as-cast Zn-Ti alloys.....	52
Figure 5.26. The average elongation to failure for the as-cast Zn-Ti alloys.....	53
Figure 5.27. Stress-strain curves for the as-extruded Zn-Ti alloys.....	56
Figure 5.28. The average ultimate tensile strength for the as-extruded Zn-Ti alloys.	58
Figure 5.29. The average elongation to failure for the as-extruded Zn-Ti alloys.	58
Figure 5.30. SEM micrograph of the fracture surface of as-cast Zn-0.01 wt% Ti.	59
Figure 5.31. SEM micrograph of the fracture surface of as-cast Zn-0.1 wt% Ti.	60
Figure 5.32. SEM micrograph of the fracture surface of as-cast a) Zn-0.3 wt% Ti and b) Zn-1 wt% Ti.....	60
Figure 5.33. SEM micrograph of the fracture surface of as-extruded Zn-0.01 wt% Ti.....	61
Figure 5.34. SEM micrograph of the fracture surface of as-extruded Zn-0.1 wt% Ti.....	62
Figure 5.35. SEM micrograph of the fracture surface of as-extruded Zn-0.3 wt% Ti.....	62
Figure A.1. Copyright permission for the Zn-Ti phase diagram from Figure 3.1a.	73

List of tables

Table 2.1. Design requirements for biodegradable stent materials.....	6
Table 4.1. Nominal compositions of the alloy samples.....	24
Table 4.2. Experimental compositions of the Zn-Ti alloys (wt%).	26
Table 5.1. Hardness test results of the as-cast Zn-Ti alloys.....	45
Table 5.2. Hardness test results of the as-extruded Zn-Ti alloys.....	47
Table 5.3. Tensile test results for the as-cast Zn-Ti alloys.	50
Table 5.4. Tensile test results for the as-extruded Zn-Ti alloys.....	54

Acknowledgements

I would like to thank my advisor, Dr. Jaroslaw Drelich for his guidance throughout this project. I could not have done it without his help and support.

I would also like to thank the other members of my committee, Dr. Jeremy Goldman and Dr. Daniel Seguin for their contributions to this research and thesis.

In addition, I would like to thank Dr. Ehsan Mostaed, Jeff Brookins, Dr. Xubo Liu, Dr. Shan Zhao and Dr. Hua-Lan Jin for their help with this project. This work would not have been completed without their support.

Finally, I want to thank Dr. Joe Licavoli for her help with the vacuum induction melting. I would also like to thank Paul Fraley for his help with the hot extrusion and the tensile testing. I would like to thank Yang Yang for his help with the use of extrusion die. I would also like to thank Owen Mills for his SEM training and his assistance with SEM. I would like to thank Dr. Edward Laitila for his help with X-ray diffraction.

Abstract

Stents made of biodegradable metallic materials are increasingly gaining interest within the biomaterials field because of their superior mechanical properties and biodegradation rates as compared to polymeric materials. Zinc and its alloys have been developed and investigated as possible candidates for biodegradable stent applications in the last five years. This study intended to formulate and characterize a new series of Zn-Ti alloys, with titanium additions of less than 1-3 wt%, with the primary objective to develop and select an alloy that meets benchmark values of mechanical properties for biodegradable stents. A series of Zn-Ti alloys was formulated through vacuum induction melting. The experimental approach was to analyze the effect of Ti alloying element addition on mechanical properties of zinc. The structure, mechanical properties and fractography of the as-cast alloys were investigated.

It was found that the grain size was reduced from above 600 μm to $\sim 23 \mu\text{m}$ with the Ti content increasing from 0.01 wt% to 0.3 wt%. The amount of the intermetallic phase increased from 0.3 wt% to 2.5 wt% with Ti content. The results identify the formation of a eutectic phase of zinc with intermetallics at the primary grain boundaries. Zn_{16}Ti was identified as the intermetallic phase formed in the as-cast Zn-Ti alloys. With increasing Ti content from 0.01 wt% to 1 wt%, the ultimate tensile strength and yield strength of the as cast Zn-Ti alloys increased from 101 and 64 MPa to 177 and 122 MPa, respectively. It is proposed that the strength of as-cast Zn-Ti alloys increases with the Ti content increasing from 0.01 wt% to 0.3 wt% due to grain refinement from a small percentage of titanium. The amount of the intermetallic phase increased with the Ti content increasing

from 0.3 wt% to 2.5 wt%. It is proposed that the hardness and strength of the as-cast Zn-Ti alloys increased with the Ti content increasing from 0.3 to 2.5 wt% due to the increased formation of Zn-Ti intermetallic phases. The low elongation of the as-cast Zn-0.3 wt% Ti (3%), Zn-0.5 wt% Ti (4%), and Zn-1 wt% Ti alloys (2%) was also attributed to the increasing content of Zn-Ti intermetallic phases.

Based on the results of the structure and mechanical properties of as-cast Zn-Ti alloys, the most promising as-cast candidates were processed through hot extrusion. This phase study was focused on the structure-property relationships before and after hot extrusion. The as-extruded Zn-0.01 wt% Ti had the highest average ultimate tensile strength and yield strength of 269 and 177 MPa, respectively. It is proposed that a significant increase in the ultimate tensile strength and yield strength in Zn-0.01 wt% Ti alloy after hot extrusion is due to grain refinement and formation of precipitates. The as-extruded Zn-0.1 wt% Ti and Zn-0.3 wt% Ti alloys exhibited high ductility, with the elongation to failure of about 44% and 30%, respectively. It is proposed that the as-extruded Zn-0.1 wt% Ti alloy exhibited high ductility due to the grain refinement and grain shape adjustment after hot extrusion. The high elongation of the as-extruded Zn-0.1 wt% Ti and Zn-0.3 wt% Ti alloys is consistent with the microstructural observations of ductile fracture. The as-extruded Zn-0.1 wt% Ti alloy had the best combination of tensile mechanical properties (UTS=207 MPa, YS=163 MPa, and Elongation=44%), which nearly meet the mechanical requirements for stent application.

1 Introduction

Coronary artery disease is the leading cause of death in the United States [1]. Coronary artery disease occurs when the arteries that supply blood to the heart and other parts of the body become narrowed. The coronary arteries become narrow due to the buildup of plaque on the inner walls of the arteries. When this happens, the blood flow to the heart decreases. Angina, shortness of breath, heart attack, or other coronary artery disease symptoms can occur if the flow of oxygen-rich blood to the heart muscle is decreased. Four treatments are used to restore and improve blood flow within arteries: drugs, arterial bypass surgery, angioplasty, and stent placement. The coronary stent has been developed to avoid many of the complications of bypass surgery for opening blocked arteries. The implantation of stents has become the most common treatment for coronary artery disease after the first widely used metallic stent was clinically evaluated and commercialized [2, 3]. Currently, coronary artery stenting is the main treatment of choice for patients with blocked coronary arteries [4, 5].

A typical coronary stent consists of a tiny mesh tube deployed into a narrowed artery and expanded in a diseased site to keep the artery open. The stent is deployed via a balloon catheter, which is withdrawn after stent deployment. When the stent expands, it fragments the rigid plaque and expands the arterial wall. This expanded stent then stays within the artery and helps restore blood flow [2].

Unfortunately, conventional stents elicit adverse long-term effects due to their permanent presence in the coronary arteries [6]. The mechanical support provided by a stent is thought to only be required temporarily during the healing process. The stents therefore

only need to retain their mechanical properties for approximately 6-12 months until the artery remodels and heals [7, 8]. After this period, arterial support is no longer needed since the artery has healed completely. In order to mitigate the long-term side effects associated with corrosion-resistant stents, a new generation of biodegradable metal stents is currently being developed. These new coronary stents will be absorbed by the body after completing their task as vascular scaffolding.

While bioabsorbable stents can potentially overcome many of the problems associated with traditional permanent stents, there are still significant research and development challenges that must be overcome for bioabsorbable stents to achieve the desired mechanical properties, biocompatibility, and degradation rates. Both polymeric and metallic materials have been investigated as candidates for bioabsorbable stents in the past [9]. Polymeric materials such as poly-L-lactic acid (PLLA), poly-D, L-lactic acid (PDLA), poly-ε-caprolactone (PCL), and polyglycolic acid (PGA) are the most extensively used in bioabsorbable stent applications due to their biocompatibility and physiological metabolites [8, 10, 11]. However, they typically have a lower strength than metals. Strut thickness of polymeric stents are necessarily larger than that of metallic stents [12]. Therefore, the use of polymeric stents is limited because of their relatively lower strengths when compared with metallic stents.

Recently, the stents made of biodegradable metallic materials are increasingly gaining interest within the biomaterials field because of their superior mechanical properties and biocompatibility rates, as compared to polymeric materials [2, 13]. Magnesium and iron alloys are biocompatible materials which have been primarily investigated as prospective candidates for stent applications during the last several years [14]. However, the most

commonly reported shortcoming of magnesium alloys is that they corrode too rapidly to provide the mechanical reinforcement during the arterial remodeling and healing period [15, 16]. Alloying elements such as aluminum, manganese and rare earth elements are added to magnesium alloys in order to reduce their corrosion rate [13, 14, 17].

Iron is also a potential candidate for biodegradable stent because of its high mechanical strength and biocompatibility. High strength is helpful in making stent struts thinner. Iron also has high ductility, which allows for the plastic deformation necessary for the construction of balloon-expandable stents [14, 18]. However, iron-based alloy stents degrade at a very slow rate. A previous study reported that pure iron based struts were still detected after 18 months during the implantation process [19, 20]. A faster degradation rate of iron is needed to meet the clinical requirement for stent implantation. The modification of the composition and geometry of the stent is needed to accelerate the degradation process.

A breakthrough in the field of biodegradable metallic stents was made in 2013 at Michigan Tech with the introduction of zinc (Zn), which degrades at a nearly ideal rate of ~0.02 mm/year, and is biocompatible [21]. Zinc exhibits near-ideal biocorrosion behavior and good antiatherogenic properties [21, 22]. However, pure zinc has a much lower strength than other metals, which is not adequate to support a diseased blood vessel [21]. The tensile strength of pure zinc is typically between 80 and 120 MPa, while a minimum of 200 MPa is required for endovascular stent applications [21]. The mechanical properties of zinc alloys need to be improved to facilitate their application as endovascular stents, either by altering the composition of alloying elements, modifying the microstructure, or both.

This research intended to formulate and study a new series of Zn-Ti alloys, with titanium additions of less than 1-3 wt%, with the primary objective to develop and select an alloy that meets benchmark values of mechanical properties for biodegradable endovascular stents.

2 Background and Literature Review

2.1 Criteria for bioabsorbable stents

Stenting has become a well-established procedure for the treatment of coronary artery occlusions [23]. Stents are delivered to the narrowed section of a coronary artery and expanded to a larger diameter by expansion of the balloon. Stents should provide mechanical reinforcement to the arterial wall during the remodeling process. This arterial support is no longer needed after the artery has healed completely. Therefore, the role of stenting is temporary, and only needed during the healing period [7, 8]. The long-term presence of the stents could trigger late complications such as restenosis and thrombosis [2].

Materials commonly used for biomedical applications can be divided into inert and resorbable. The resorbable materials are progressively absorbed by the body, and during the degradation process the mechanical strength and stiffness of the materials decrease. Inert materials remain at the implantation site for a life time, which can have adverse long-term consequences [24]. Permanent stents are made of 316L stainless steel, Nitinol and cobalt-chromium alloys. Those alloys can provide relatively high strength and good corrosion resistance. However, permanent metallic stents have several drawbacks, which limit their widespread use. Some of these limitations include long-term endothelial dysfunction, late thrombosis, delayed re-endothelialization, thrombogenicity, permanent physical irritation, chronic inflammatory local reactions [25]. A bioabsorbable stent can potentially overcome many of the shortcomings of permanent stents [9]. Therefore,

bioabsorbable stents are designed to support the arterial wall during the remodeling and to degrade thereafter.

In order to fabricate suitable biodegradable stents, a series of requirements must be satisfied for the candidate stent materials. The material for biodegradable stents needs to meet the mechanical and biological specifications listed in Table 2.1, while still remaining able to be eliminated from the body after accomplishing its function.

Polymeric materials are one of the suitable candidates to be used as stent materials due to their biocompatibility and physiological metabolites [8, 10, 11]. However, the low mechanical strength of polymeric materials may inhibit its use. Metallic materials show several important advantages over polymeric materials. Three metallic materials including iron, magnesium, and zinc have been investigated for cardiovascular stent applications.

Table 2.1. Design requirements for biodegradable stent materials.

Properties	Constraints
Mechanical Integrity	> 6-12 months [14]
Biocompatibility	Non-toxic and non-inflammatory [26]
Yield Strength	> 200 MPa [26]
Ultimate Tensile Strength	> 300 MPa [26]
Elongation to Failure	> 15-18% [26]
Fatigue Strength at 10^7 cycles	> 256 MPa [21]
Elastic Recoil on Expansion	< 4% [26]
Hydrogen Evolution	< $10 \mu\text{L H}_2 \text{ cm}^{-2} \text{ day}^{-1}$ [27]
Corrosion rate	$\sim 0.02 \text{ mm year}^{-1}$ [28]

2.2 Biodegradable iron and magnesium materials for stent application

Iron (Fe) and magnesium (Mg) based alloys have been investigated as the candidates for biodegradable stents in the past, mainly in the last two decades [14]. Fe is needed for the

synthesis of proteins and Fe-containing enzymes production in human body [29]. It functions mainly in the reduction of ribonucleotides, the transport, storage and activation of oxygen, and other electron transport [30]. Peuster et al. [20] first investigated the *in vitro* and *in vivo* degradation of pure iron scaffolds (> 99.8% iron) in 2001. No thromboembolic complications and no adverse events occurred during the follow up of 6-18 months after implantation of degradable iron stents. This study proposed that degradable iron stents can be safely implanted without significant obstruction of the stented vessel caused by inflammation response, neointimal proliferation, or thrombotic events. However, pure iron struts were still detected after 18 months during the implantation process because of the slow degradation rate. Based on the requirements provided in Table 2.1, a much faster degradation rate is desirable for iron in physiological environments. Iron also accumulates a voluminous corrosion product that repels neighboring cells and biological matrix [31].

In order to increase the degradation rate for pure iron, several previous investigations have been performed on the development of alloys or microstructures while maintaining its appropriate mechanical properties. Hermawan et al. [32-35] first studied the effect of alloying element Mn on the properties of iron for biodegradable stents. A series of Fe-based alloys with additions of Mn (20, 25, 30, and 35 wt%) were designed. The results indicated that Fe based alloys have higher corrosion rate compared to that of pure Fe. The Fe-35 wt% Mn alloy showed mechanical properties and degradation behavior closely approaching those required for biodegradable stents application. This study also determined that the microstructures of the Fe-Mn alloys mainly consisted of γ phase and

ϵ phase, which decreased the magnetic susceptibility. As a result, the Fe-Mn alloys became compatible with the magnetic resonance imaging (MRI).

Moravej et al. [36, 37] developed pure iron foils with a fine grain microstructure, suitable mechanical properties, and moderate corrosion rate using an electroforming method. This study indicated that electroformed pure iron has a faster degradation rate than pure iron fabricated by a casting method. This work also proposed that electroformed pure iron did not result in a decrease in metabolic activity when exposed to primary rat smooth muscle cells. However, it caused a decrease in the cell proliferation activity, which would have a beneficial effect on the inhibition of in-stent restenosis.

Liu et al. [38] investigated the effect of alloying elements such as Mn, Co, Al, W, Sn, B, C, and S in binary Fe-X alloys on biodegradability and biocompatibility of iron for biodegradable stents. The results indicated that the addition of Mn, Co, W, B, C, and S improved the yield and ultimate strength of iron in the as-rolled materials, whereas the alloying element Sn caused a severe reduction in the mechanical properties. Additionally, it was found that the corrosion rates of pure iron and the Fe-X binary alloys were of the same order of magnitude. Extracts from the pure iron and all Fe-X binary alloys (except for the Fe-Mn alloy), decreased the cell viabilities of L929 cells and VSMC compared with 316L SS but showed no significant cytotoxicity to ECV304 cells. This study also determined that most of the platelets, which adhered to the surface of the Fe-X binary alloys were round, with no sign of thrombogenicity. In conclusion, the elements Co, W, C, and S were found to be suitable as alloying elements for iron based on a comprehensive consideration of the improved mechanical properties, appropriate corrosion rates and good biocompatibility. High content alloy additions and multi-

component iron alloys were recommended to improve corrosion performance of iron in future.

Magnesium has also shown considerable promise for biodegradable stent materials because of its good biocompatibility and low thrombogenicity. The use of magnesium as a biodegradable stent material was also based on the fact that it is a structural constituent of the tissue and essential element in the human body [14]. Magnesium has been proven cytocompatible by previous investigations including an indirect contact cytotoxicity test involving sterilized pure Mg and Mg-Ca alloys using L-929 cells [39, 40]. However, pure magnesium usually has a fast degradation rate in aggressive chloride environments such as human body fluid [40]. The rapid degradation of the magnesium stents can lead to restenosis and loss of mechanical integrity, which can limit its application as an implant material [41]. In order to decrease the degradation rate of magnesium, alloying with other elements and novel fabrication methods were explored [17].

Heublein et al. [42, 43] first investigated the degradation behavior of magnesium alloys in an endovascular environment. Magnesium alloy AE21 (containing 2% aluminum and 1% rare earths) was used during an animal study and a mass loss of only 50% was reported during six months. The experiments were performed by implantation of stents into the coronary artery of eleven domestic pigs. The results indicated that there was no platelet deposition or thrombus at the endothelial sites after any of the assessment intervals. A negligible inflammatory response was observed. However, the degradation occurred faster and the loss of mechanical integrity occurred only between 35 and 56 days after implantation. Further improvements are necessary to slow down the degradation rate and maintain mechanical integrity.

Schranz et al. [44] studied the implantation of magnesium alloy vascular scaffolds in the aorta of a 3-week old male patient to treat recoarctation of the aorta. This study observed that the vessel begins to return to its original damaged state upon degradation of the magnesium vascular scaffold. The absorption rate of the magnesium alloy was still too rapid to support the vessel during the healing process. Based on the results of coronary stenting with absorbable magnesium stents trial, the vascular scaffold was completely absorbed within two months. These vascular scaffolds were associated with a high restenosis rate, but no deaths, thrombosis, or heart attacks were reported in this study. The results of this study proved that magnesium vascular scaffolds are biocompatible. However, many magnesium alloys lost their mechanical strength too quickly because of their rapid resorption rate, causing vessel recoil during the healing process [45].

Waksman et al. [46] evaluated the degradation rate and long-term vascular responses to the absorbable magnesium stent. In this work, the PROGRESS-AMS was a prospective, multicenter clinical trial of 63 patients with coronary artery disease who received absorbable magnesium alloy stents prototyped by BIOTRONIK AG in Zurich, Switzerland. The results indicated that the scaffolds were nearly completely degraded at four months, with no adverse effects to the vessel wall. Slower degradation is required to provide sufficient radial force of the stent to improve long-term patency rates of the absorbable metal stent.

Hanzi et al. [47-49] developed new bioabsorbable magnesium alloys ZW21 and WZ21 containing other alloying elements such as Zn, Y, Ca, and Mn. The magnesium alloys had fine and even microstructures with grains smaller than 10 μm , which generated exceptional plasticity of 17% and 20% at ambient temperature. Therefore, it makes them

interesting candidates for stent application. The results also indicated that these alloys exhibited homogeneous degradation behavior in physiologically simulated solutions, which have higher resistance to corrosion than that of other magnesium alloys.

2.3 Zinc-based alloys for biodegradable stents

Zinc based alloys have been developed and investigated as possible candidates for bioabsorbable stent applications due to their nearly ideal biodegradation rate and acceptable biocompatibility [21]. Zinc is an essential element for biological functions in nucleic acid metabolism, signal transduction, apoptosis regulation, gene expression, and endocrine regulation apart from interacting with a wide range of organic ligands [50, 51]. Zinc could potentially reduce the major problem of in-stent restenosis, which can cause stent implant failure [52].

The degradation of iron was found to be too slow, while the degradation rate of magnesium is too fast as a potential biodegradable material for stent applications. The degradation problem associated with Mg and Fe could be avoided by using zinc and its alloys. Zinc exhibits near-ideal biocorrosion behavior and good antiatherogenic properties [21, 22]. Zinc has a standard corrosion potential of -0.8 V (vs SCE), intermediate between Fe (-0.4 V) and Mg (-2.4 V) [53], making this metal electrochemically more noble than Mg and more active than Fe. Zinc can provide antiatherogenic properties by preventing metabolic physiologic derangements of the vascular endothelium, which appears to be crucial for the protection against cell destabilizing agents such as polyunsaturated lipids and inflammatory cytokines [22]. However, pure zinc has a much lower strength than other metals such as magnesium and

iron. The tensile strength of pure zinc is <80-120 MPa, while a tensile strength of at least 200 MPa, preferable close to 300 MPa is required for the cardiovascular stent application [21]. In recent years, several new biodegradable zinc based alloys have been developed to improve the mechanical properties of zinc alloys in order to facilitate their application as endovascular stents, either by altering the composition of alloying elements or by modifying the microstructure.

Vojtěch et al. [54] developed Zn-based alloys containing up to 3 wt% Mg as potential biodegradable materials for medical use. In this work, the structure, mechanical properties and corrosion behavior of Zn-Mg alloys were studied. The results indicated that the tensile strength of the as-cast Zn-Mg alloys increased from 30 MPa to 150 MPa with the Mg content increasing up to 1 wt%. A relatively fine structure composed of primary zinc and an interdendritic eutectic mixture formed with additions of Mg, and this may have contributed to the increase in the tensile strength of the as-cast Zn-Mg alloys. However, the maximum elongation of the as-cast Zn-Mg alloys was only 2%, which would not be enough for stent application [21]. The results of this study also indicated that the Zn-Mg alloys had corrosion rates that ranged from 0.05 to 0.1 mm/yr, when immersed in a simulated body fluid with a pH of 7. The influence of Mg on the corrosion rate of the Zn-Mg alloys is small because of the low Mg concentrations used in this study.

Additional improvements in mechanical properties of Zn-Mg alloys can be achieved by hot extrusion. Mostaed et al. [55] investigated novel Zn-Mg alloys for biodegradable stent applications. Pure Zn and four Zn-based binary alloys with Mg contents ranging from 0.15 to 3 wt% were developed by casting process and homogenized at 350 °C for 48

hr followed by hot extrusion at 250 °C. It was determined that the ultimate tensile strength of the extruded Zn-Mg alloys increased from 250 ± 9 MPa to 399 ± 14 MPa with the Mg content increasing from 0.15 to 3 wt%. For Zn-based binary alloy with 3 wt% Mg addition, the ultimate tensile strength increased by 260% as compared to that of pure Zn. However, the elongation to failure dramatically dropped from 60% to 0.8% moving from pure Zn to Zn-3 wt% Mg. The lack of ductility for Zn-3Mg restricts its use in biodegradable stent applications. The investigations revealed that increasing the Mg content improved micro-hardness and tensile strength of the Zn-Mg alloys because of the increasing volume fraction of the hard Mg_2Zn_{11} intermetallic phase. The presence of hard and brittle Mg_2Zn_{11} intermetallic particles can also lead to the easy nucleation and growth of cracks. Therefore, a corresponding decrease in ductility also occurred. The results of this study also indicated that the corrosion rates of Zn and Zn-Mg alloys in both as-cast and extruded conditions were in the same order of magnitude (from 0.12 to 0.18 mm/yr). Extruded Zn-Mg alloys exhibited slightly superior corrosion resistance and a slower degradation ratio than those of their as-cast conditions because of the formation of Mg_2Zn_{11} phase. The Mg_2Zn_{11} phase has the highest corrosion resistance among Zn-Mg phases [56]. The difference in corrosion rates between the Zn-Mg alloys and pure Zn is not significant.

The results of work by Mostaed et al. [55] are consistent with the findings of Kubásek et al. [57]. The results of their study demonstrated that the hardness and strength increased with increasing Mg concentration when Zn-(0-1.6 wt%) Mg alloys were prepared by hot extrusion at 300 °C. The hot extruded Zn-0.8 wt% Mg alloys had the best combination of tensile strength (301 MPa) and elongation (15%) among all the investigated Zn-Mg

alloys. In this work, the Zn-1.6 wt% Mg alloy had elongation of near zero because of the presence of continuous hard and brittle Mg_2Zn_{11} intermetallic phases. For Zn-(0-1.6 wt%) Mg alloys, increases of Mg concentration resulted in decreasing plasticity of alloys [57]. Alloying is a general and effective method to improve the mechanical properties as well as the corrosion resistance of Zn-based alloys. Some investigations have focused on this approach to Zn-Mg based alloys, such as the addition of manganese (Mn), strontium (Sr), and calcium (Ca). Manganese has no toxic effects and plays an important role in the activation of multiple enzyme systems, which has much effect on corrosion behaviors by removing and avoiding introducing the heavy-metal elements during casting process [58, 59]. Strontium (Sr) and calcium (Ca) are essential elements for cell chemical signaling and involve in mineralization, enzymatic reactions in human body [60]. The addition of strontium (Sr), and calcium (Ca) to Zn has been investigated by Li et al [61, 62]. The results of their study indicated that Sr and Ca could improve both mechanical strength and hardness of pure Zn. The elongation of as rolled Zn-1 wt% Sr binary alloy were further improved up to $20\pm 2\%$. However, the elongation of as rolled Zn-1 wt% Ca was still low in spite of a significant improvement for pure Zn with an initial $0.32\pm 0.08\%$ elongation.

Liu et al. [63] studied the effect of the alloying element Mn on the mechanical properties, *in vitro* degradation behaviors, and hemocompatibility of the Zn-Mg alloy. In this work, the Zn-Mg-Mn alloys were prepared with composition of Zn-1Mg-0.1Mn and Zn-1.5Mg-0.1Mn. The results indicated that the yield strength, ultimate tensile strength, and elongation of as rolled Zn-1Mg-0.1Mn alloy were 195 MPa, 299 MPa, and 26%, which were largely improved compared to pure Zn. The results of this study also showed that

the as rolled Zn-1Mg-0.1Mn alloy possessed appropriate corrosion rate of 0.25 mm/year during immersion in Hank's solution. In addition, the results of hemolysis rate and platelet adhesion indicated that the as rolled Zn-1Mg-0.1Mn alloy had lower hemolysis rate of 1.1% and no signs of thrombogenicity with excellent blood compatibility. Liu et al. [64] also developed novel Zn-1.5Mg-0.1Sr ternary alloy as new biodegradable implant materials. The results revealed that the ternary alloys had much higher yield strength, ultimate tensile strength and elongation than those of Zn-1.5Mg alloy. The ternary alloy was composed of the matrix Zn and precipitated phases Mg_2Zn_{11} and $SrZn_{13}$, and their grain size became more homogeneous and smaller compared to that of Zn-1.5Mg alloy. Compared to Zn-1.5Mg alloy, it was determined that addition of Sr decreased the size of coarse primary dendrites in this work. The results revealed that the corrosion rate of the ternary alloy was significantly higher than that of Zn-1.5Mg alloy. In this study, the novel Zn-based ternary alloys provided the ideal values of corrosion rate for potential bioabsorbable materials use in stent applications.

There are few other studies of Zn based binary alloys such as Zn-Al, Zn-Li, and Zn-Cu as new potential materials for biodegradable implants [65-67]. Mostaed et al. [55] investigated two Zn-Al binary alloys as potential biodegradable materials for stent applications, which were developed by casting process and homogenized at 350 °C for 48 hr followed by hot extrusion at 250 °C. The results indicated that addition of Al leads to improvement of yield strength and ultimate tensile strength to 119 and 203 MPa for extruded Zn-0.5Al, and to 134 and 223 MPa for extruded Zn-1Al, respectively, which had also remarkably high fracture elongation of 33% and 25%. The difference between the Zn-Al binary alloys and pure Zn was very small in this study. However, the toxicity

related concerns for Zn-Al alloys restrict them from stent applications. There is still disagreement on the subject of aluminum as an allowable alloying addition. Bowen et al. [66] indicated that no local toxicity was identified over a range of Al content up to 5.5 wt% Al, which were developed and implanted in rats in search of new alloys with possible applications as bioabsorbable endovascular stents.

2.4 Novel Zn-Ti Alloys for medical application

Titanium has no toxic effects and is considered as a highly biocompatible metal [68, 69]. Titanium and its alloys are one of the most commonly used metals and alloys for medical device applications [70]. Titanium and its alloys are suitable for load bearing implants due to their superior mechanical properties, chemical stability, and biocompatibility under *in vivo* conditions [71-73]. The toxic potential of a Zn-Ti stent should be negligible in this study. The recommended dietary allowance for zinc and titanium are 10 and 0.8 mg/d, respectively [74, 75]. The weight of an endovascular metallic stent is ~50 mg. For an alloy of Zn-2.5 wt% Ti, the total mass of Zn and Ti are 48.75 mg and 1.25 mg. The daily release of Zn and Ti into biological system are 134 μg and 3 μg , respectively, if the stent degrades completely within one year. The estimated daily dose of elements from a Zn-Ti stent are far less than the recommended daily values [21, 65]. Therefore, the systemic toxicity of a Zn-Ti stent should be nonexistent.

There have been no systematical investigations of Zn-Ti binary alloys for biomedical applications. Selection of Ti as an alloying element is motivated by differences in microstructure recorded for Zn wires made of high purity (HP) and commercially pure (CP) Zn, which were extruded and drawn with a collaborating institution in Germany

(Figure 2.1). The major difference between the HP and CP Zn materials is the Ti level (0.05 wt%, in CP versus almost none in HP). This difference in Ti content likely accounts for the refined microstructure of the Zn. Other impurities (most of which were higher in the CP Zn) could have also contributed to the grain refining effect.

As is well known, titanium is a common alloying element in industrial steels [76].

Titanium in low carbon steels can form intermetallic precipitates that provide grain refinement and precipitation strengthening. Titanium acts as a solution atom or precipitation to suppress the recrystallization and grain growth of austenite. The fine-grained microstructure can improve the strength and toughness of steels. Microalloying titanium in steels can lead to the formation of titanium precipitates, which can further influence the properties [77-80].

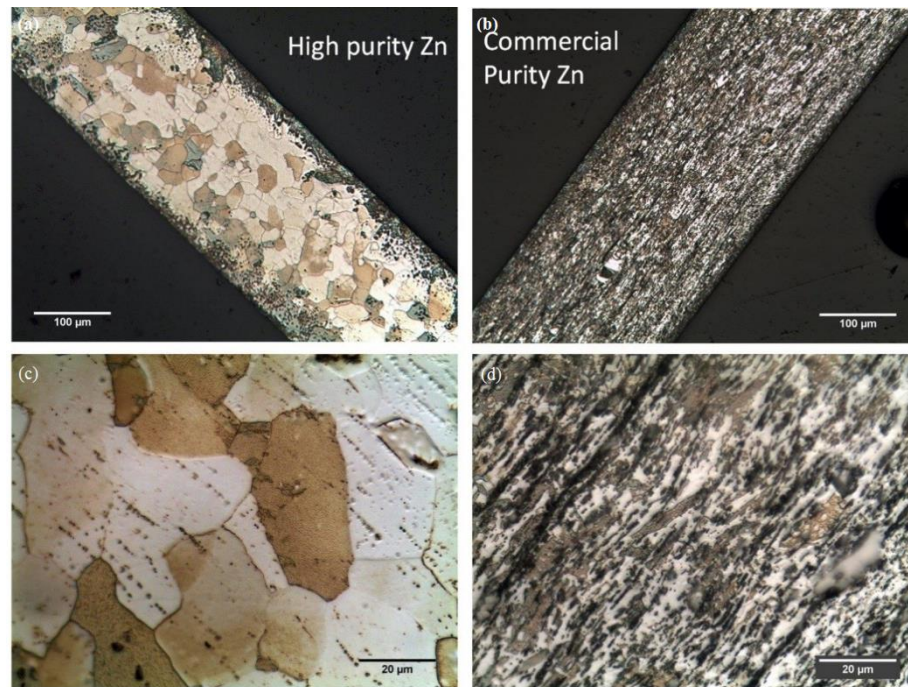


Figure 2.1. Optical micrographs for high purity (HP) and commercial purity (CP) zinc wires.

Titanium is often added to aluminum alloys because of its potential grain refining effect. Jaradeh et al. [81] studied the effect of Ti content on the solidification structures of aluminum alloys of AA3003 type. The results revealed that the AA3003 alloys with Ti additions (<0.02%) had the finest grain structure. However, the grains were coarser with Ti content increasing up to around 0.15%. Saheb et al. [82] investigated the influence of Ti addition (up to 4 wt%) on wear behavior of as-cast and heat-treated Al-12 wt% Si eutectic alloy. The results indicated that the addition of Ti to the binary Al-Si alloy led to the precipitation of the intermetallic compound Al_3Ti phase, which induced an increase in the microhardness of the binary alloy. Li et al. [83] investigated the effect of Ti alloying element on the microstructural and mechanical properties of Cu-40Zn brass. The results of this study showed that remarkable grain-refinement and strengthening effects were achieved by the addition of Ti to Cu-40Zn brass. However, it was found that Ti segregated in the primary particle boundaries at elevated temperatures, which significantly deteriorates the mechanical properties of the Cu-40Zn-1Ti. Leone et al. [84] studied the effect of titanium concentration on the effectiveness of grain refinement in Zn-Ti alloy. This work observed that addition of a small percentage of titanium (0.1 wt%) to zinc resulted in grain refinement. The number of zinc-rich grains increased with increasing the titanium concentration. However, too much titanium resulted in coupled and primary intermetallic phase growth. The addition of Ti caused strong precipitation hardening of alloy with the formation of intermetallic phase [85, 86]. Based on the current analysis and the above literature review, alloying with titanium is expected to provide beneficial effects on the mechanical properties of zinc.

3 Goals and Hypotheses

In this study, a series of Zn-Ti alloys with Ti content less than 3 wt% was formulated through vacuum induction melting. The effect of addition of the alloying element Ti on structure and mechanical properties of a base alloy of zinc was studied. Based on the results of the structure and mechanical properties of as-cast Zn-Ti alloys, the most promising as-cast candidates were studied after hot extrusion with the primary goal of exploring suitability of Zn-Ti alloys as biodegradable metals for vascular stenting applications. In this research, studies were planned to investigate new Zn-Ti alloys aiming to have: i) a tensile strength of at least 200 MPa, preferably close to 300 MPa, which have enhanced tensile strength as compared to pure zinc (<80-120 MPa), and ii) an elongation to failure of at least 15%, preferably above 20% [26].

The Zn-rich part of the Zn-Ti binary phase diagram is presented in Figure 3.1, which is carried out in the concentration area of the Zn-rich alloys containing up to 11.0 at% (8.3 wt%) Ti [87]. As illustrated in the Zn-Ti binary phase diagram (Figure 3.1), the solid solubility of titanium in zinc is very limited and the $Zn_{16}Ti$ intermetallic phase forms with a small addition of Ti. Based on the phase diagram, it was hypothesized that the addition of titanium to zinc could be used to facilitate precipitation hardening and solid solution strengthening. Several Zn-Ti alloys with Ti contents ranging from 0.01 to 2.5 wt% (0.014 to 3.4 at%) were selected for this study to explore the effect of Ti content on mechanical characteristics of the Zn-Ti binary system. By keeping a low content of Ti, we aimed to control both the Zn rich solid solution and $Zn_{16}Ti$ intermetallic phases. The formation of the $Zn_{16}Ti$ intermetallic phase can cause strong hardening of Ti in Zn-Ti alloys [85, 86].

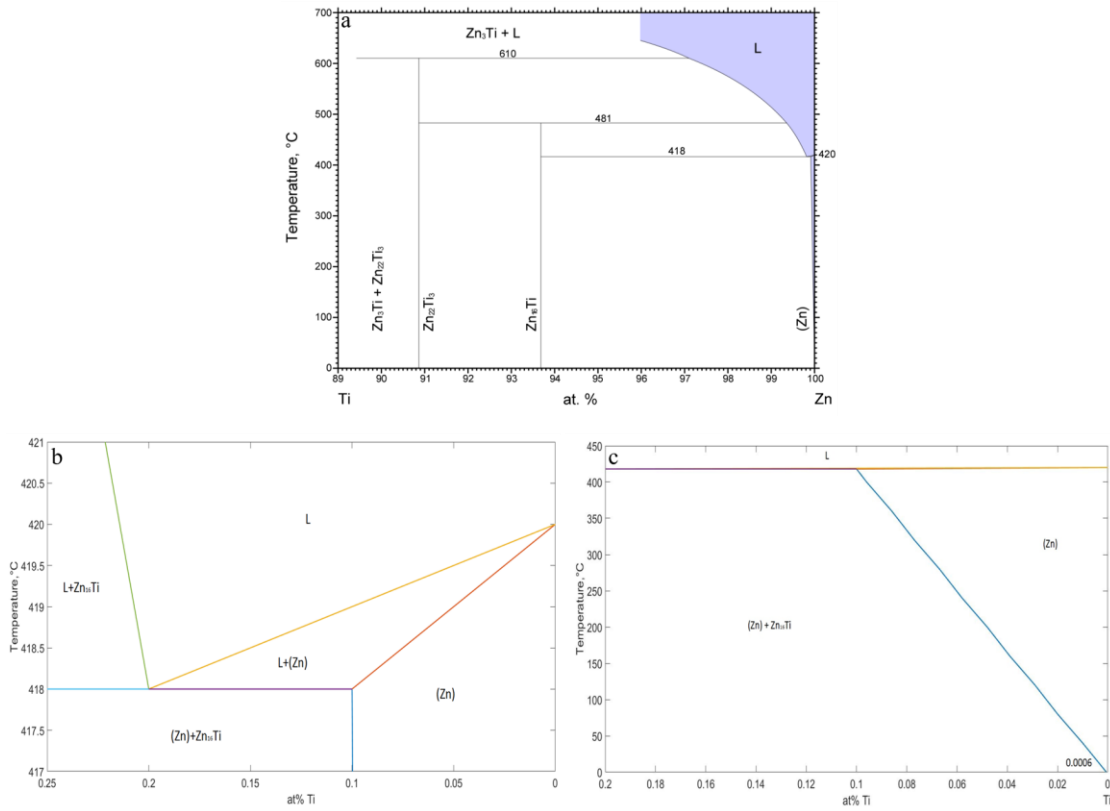


Figure 3.1. Zn-Ti binary phase diagram: a) 89-100 at% Zn [87], b) Temperature from 417 to 421 °C, c) Ti content from 0 to 0.2 at% (estimate based on Ref. [87, 88]).

Hypothesis 1: *The mechanical strength of as-cast Zn-based alloys can be improved with the Ti content increasing from 0.01 wt% to 2.5 wt% because of the strengthening by intermetallic phases.*

As illustrated in Zn-Ti binary phase diagram (Figure 3.1), the solid solubility of titanium in zinc is very limited. Anderson et al. indicated that the solubility of Ti in Zn as 0.01 to 0.02 at% (0.007 to 0.015 wt%) at 300 °C [87]. Heine et al. concluded the solubility of Ti in Zn at the room temperature to be less than 0.0005 wt% (0.0006 at%) [88]. For solid solution type, a substitutional solid solution or an interstitial solid solution can form

depending on the relative difference in atomic radii. The relative difference in atomic radii between Ti (1.47×10^{-10} m) and Zn (1.39×10^{-10} m) is small [89]. It is proposed that the point defects in the zinc crystals are either substitutional or interstitial when titanium solute atoms are added to zinc. Titanium solute atoms cause lattice distortions, impeding dislocation motion and increasing the yield stress of the Zn-Ti alloys, which leads to an increase in strength of the Zn-Ti alloy. In general, the strength of Zn-Ti alloys can be increased by increasing the concentration of the titanium solute atoms [89]. However, there is a very low limit to the amount of titanium solute that can be added in this study. Based on the Zn-Ti binary phase diagram (Figure 3.1), the $Zn_{16}Ti$ intermetallic phase forms when the alloying element Ti is at concentrations above its solubility limit. In this study, it was predicted that the final phases of studied Zn-Ti alloys are Zn-rich solid solution phase and $Zn_{16}Ti$ intermetallic phase. Intermetallics are almost always very hard and brittle, which are formed by combining two or more metallic elements. Intermetallics are similar to ceramic materials in terms of their mechanical properties [90]. It is possible that an energy barrier to dislocation motion results from the strain field caused by the mismatch between intermetallics and the surrounding matrix. The energy of moving dislocations may be altered when it enters intermetallics with a different modulus than the matrix [91]. These hard intermetallics impede the movement of dislocations and the Zn-Ti alloys becomes harder and stronger. Therefore, it is predicted that the Zn based alloys can be strengthened by the intermetallic phases.

Hypothesis 2: *The improvements in the mechanical strength and restoration of ductility can be achieved for Zn-Ti alloys after hot extrusion process due to the grain refinement during hot extrusion process.*

For hot extrusion process, deformation is achieved at a temperature above that which recrystallization occurs. Hot extrusion is found to be useful in reducing casting defects, refining and homogenizing the microstructure, and breaking the eutectic networks. The mechanical strength and plasticity of the materials can be improved by all of these modifications [54]. During hot extrusion, the dynamic recrystallization then results in a significant grain refinement because of the formation of new equiaxed grains and rows of intermetallics phases [57].

4 Experimental Methods and Materials

4.1 Materials Preparation

4.1.1 Materials

In this work, pure Zn granules and pure Ti turning were melted in an inert atmosphere.

The pure Zn granule was 99.99% purity and the pure Ti rod was 99.7% purity. Both materials are supplied by Alfa Aesar (Ward Hill, MA).

4.1.2 Vacuum Induction Melting

A vacuum induction melting furnace (Figure 4.1) at Michigan Technological University was used to fabricate six different Zn-Ti alloys. Nominal compositions of the alloys are listed in Table 4.1.



Figure 4.1. Vacuum induction melting furnace.

Table 4.1. Nominal compositions of the alloy samples.

Alloy	Ti (wt%)	Zn (wt%)
Zn-0.01Ti	0.01	Bal.
Zn-0.1Ti	0.1	Bal.
Zn-0.3Ti	0.3	Bal.
Zn-0.5Ti	0.5	Bal.
Zn-1Ti	1	Bal.
Zn-2.5Ti	2.5	Bal.

Zn granules and Ti turnings (or chips) were weighed, mixed, and added to the zirconia crucible. The zirconia crucible and 304 stainless steel mold were placed in the appropriate positions and aligned. The chamber was evacuated to 15-25 mTorr under rough vacuum, then to 150-250 μ Torr under high vacuum (diffusion pump), and then backfilled with high-grade (99.998%) Ar to ~500 Torr. Melting was conducted at ~500 °C for 10-20 min. The melts were poured into a 304 stainless steel mold at ~600 °C. The ingots obtained with a diameter of ~38 mm and a height of ~60 mm (Figure 4.2).



Figure 4.2. Zn-Ti alloy ingot

4.1.3 Hot Extrusion

A system setup used in the hot extrusion process is shown in Figure 4.3, which was used to extrude Zn-Ti alloys. The extrusion die configuration is given in Figure 4.4. The as-cast ingots were homogenized at 370 °C for 1 h, followed by water quenching. The as-cast Zn-Ti alloys were subsequently hot extruded at 250 °C with an extrusion ratio of 9:1 and an extrusion speed of 15 mm/min to fabricate rods with a diameter of 6.35 mm (Figure 4.5).



Figure 4.3. System setup used in the hot extrusion process.



Figure 4.4. The extrusion die configuration.

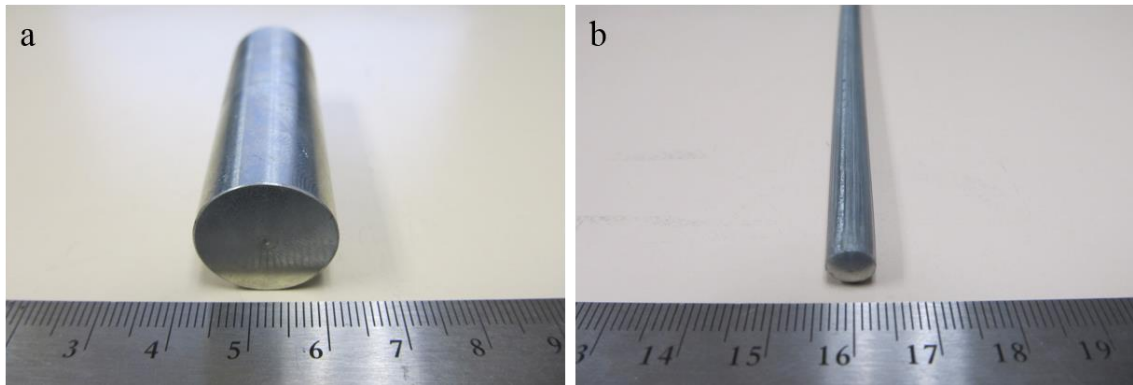


Figure 4.5. Samples of Zn-Ti alloy rod: a) before and b) after hot extrusion.

4.2 Elemental Analysis

The elemental composition of the Zn-Ti alloys was analyzed using a Perkin Elmer Optima 7000DV ICP-OES. Experimental compositions of the alloys are listed in Table 4.2.

Table 4.2. Experimental compositions of the Zn-Ti alloys (wt%).

Alloy	Ti (Experimental)	Al	Cu	Fe	Pb	Zn
Zn-0.01Ti	0.009	0.000	0.001	0.001	0.002	Bal.
Zn-0.1Ti	0.087	0.000	0.001	0.000	0.003	Bal.
Zn-0.3Ti	0.299	0.000	0.000	0.001	0.003	Bal.
Zn-0.5Ti	0.505	0.001	0.000	0.002	0.003	Bal.
Zn-1Ti	0.810	0.001	0.001	0.002	0.002	Bal.

4.3 Microstructural Analysis

The Zn-Ti alloy samples were sectioned, mounted, ground, and polished prior to microstructural analysis. The samples were sectioned and then mounted in epoxy. The sectioned samples were successively ground on 240, 360, 600 grit sand paper. The samples were then polished using 1 μm diamond paste and 0.05 μm alumina slurry. The sample was etched in Palmerton's reagent, which consists of 200 g CrO_3 , 15 g Na_2SO_4 , 1000 ml H_2O . The microstructures of the studied alloys were analyzed using an optical microscopy and a JEOL JSM-6400 Scanning Electron Microscope (SEM) with an energy dispersive spectrometer (EDS).

4.4 X-ray Diffraction (XRD)

X-ray diffraction (XRD) was performed on an XDS2000 θ/θ X-ray diffractometer (Scintag Inc., Cupertino, CA) with $\text{CuK}\alpha$ radiation ($k = 1.540562 \text{ \AA}$). The scans were performed continuously from 20 deg to 90 deg in 2θ at a speed of 0.4 deg/min with a step size of 0.02 deg.

4.5 Mechanical Testing

4.5.1 Microhardness Measurement

Vickers microhardness (HV) was measured using a LECO M-400-G1 digital hardness tester, which applied a load of 200 g and a dwelling time of 15 s. A total of 10 indentations were tested at each condition. The error bars represent the standard deviation for the 10 repeat measurements.

4.5.2 Tensile Testing

Tensile tests were performed at room temperature using an Instron 5984 electro-mechanical testing machine. The crosshead speed was 2 mm/min for all of the shear tests and all tests were performed using strain rates of 0.00208 s^{-1} . The ingots for tensile test were machined into tensile testing specimens with the gage length of $16.0 \pm 0.1 \text{ mm}$ and the diameter of $4.0 \pm 0.1 \text{ mm}$ according to ASTM E8/E8M-11 [92].

5 Results and Discussion

5.1 Microstructural Characterization

The microstructures of as-cast and as-extruded Zn-Ti alloy samples were analyzed using an optical microscopy (OM) and a scanning electron microscope (SEM) with an energy dispersive spectrometry (EDS). X-ray diffraction (XRD) was used to characterize the structures of the formulated alloys.

5.1.1 As-cast Alloys

Zn-0.01 wt% Ti: Figure 5.1 shows the optical micrographs of the as-cast Zn-0.01 wt% Ti alloy. It can be observed that the as-cast Zn-0.01 wt% Ti alloy contains large grains (above 600 μm). In a previous study, it was observed that as-cast pure Zn has very coarse grains (above 1 mm) [55, 93]. The grain size of the as cast Zn-0.01 wt% Ti alloy are smaller than that of pure Zn. This indicates that the addition of alloying element Ti can modify the microstructure and decrease the grain size of pure Zn. The grains of the Zn-0.01 wt% alloy are near equiaxed. The optical micrographs of as-cast Zn-0.01 wt% Ti alloy revealed a structure mainly composed of Zn solid solution with a small amount of Ti. As illustrated in the Zn-Ti binary phase diagram (Figure 3.1), it is proposed that the Zn-0.01 wt% Ti alloy is mainly composed of the Zn solid solution phase due to the relatively low titanium concentration in the alloy.

The X-ray diffraction patterns of as-cast Zn-0.01 wt% Ti alloy are shown in Figure 5.2. An analysis of the peaks confirmed the presence of the Zn phase in the as-cast Zn-0.01 wt% Ti alloy. This X-ray diffraction result agrees with the observations from optical

microscopy, that the as-cast Zn-0.01 wt% Ti alloy is mainly composed of the Zn phase due to the relatively low titanium concentration in the alloy.

Zn-0.1 wt% Ti: Figure 5.3 shows an optical micrograph of the as-cast Zn-0.1 wt% Ti alloy. The grain size of the as cast Zn-0.1 wt% Ti alloy is smaller than that of Zn-0.01 wt% Ti alloy. The grain size for zinc alloy decreased from above 600 μm to about 87 μm with the Ti content increasing from 0.01 wt% to 0.1 wt%. As illustrated in the Zn-Ti binary phase diagram (Figure 3.1), the Zn-0.1 wt% Ti alloy is hypoeutectic. It is proposed that the Zn-0.1 wt% Ti alloy consists of primary Zn dendrites and a eutectic of Zn and intermetallic phase mixtures.

The SEM micrograph of as-cast Zn-0.1 wt% Ti alloy is presented in Figure 5.4. SEM analysis revealed a lamellar eutectic structure at the boundaries of the Zn-0.1 wt% Ti alloy.

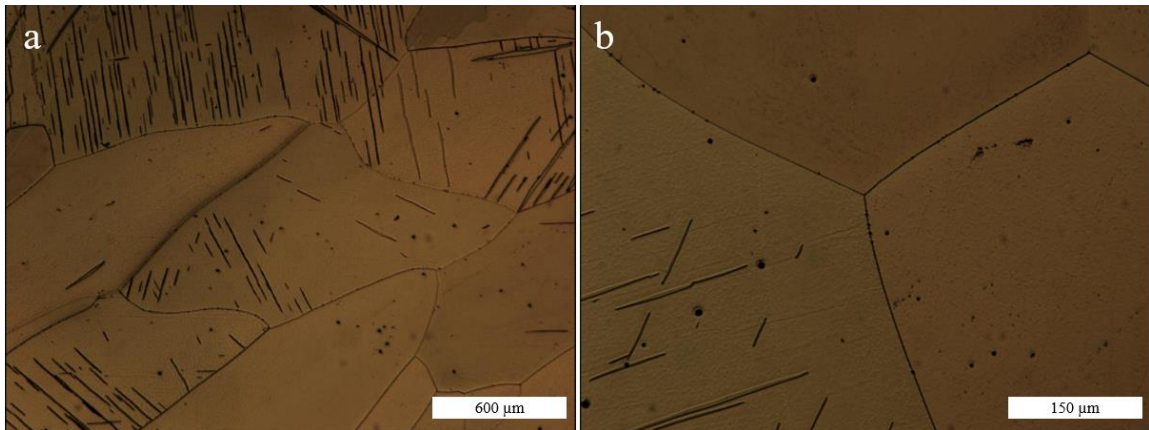


Figure 5.1. Optical micrograph of as-cast Zn-0.01 wt% Ti: a) 25x, b) 100x.

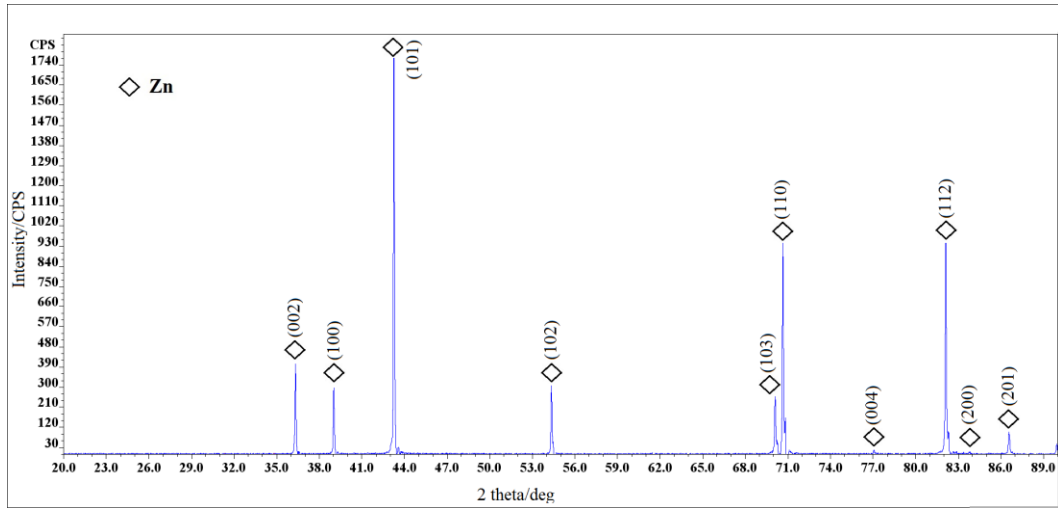


Figure 5.2. X-ray diffraction patterns of as-cast Zn-0.01 wt% Ti alloy.

Zn-0.3 wt% Ti: Figure 5.5 shows the optical micrograph of an as-cast Zn-0.3 wt% Ti alloy sample. The grain size of as-cast Zn-0.3 wt% Ti alloy is smaller than that of as-cast Zn-0.1 wt% Ti alloy. The grain size for the zinc alloy decreased from about 87 μm to 23 μm , with the Ti content increasing from 0.1 wt% to 0.3 wt%. Similar to the as-cast Zn-0.1 wt% Ti alloy, Zn grains and a eutectic of Zn and intermetallic phases mixture were observed for the as-cast Zn-0.3 wt% Ti. Primary Zn-Ti intermetallic phases were observed in the as-cast Zn-0.3 wt% Ti alloy, which was found to have a faceted structure. The EDS analysis confirmed that Zn-Ti intermetallic phases were formed in the as-cast Zn-0.3 wt% Ti alloy. The Zn-Ti intermetallic phase is approximately 96 wt% Zn and 4 wt% Ti, which is approximately 94 mol% Zn and 6 mol% Ti (Figure 5.6). EDS point scan analysis determined that the approximate mole ratio for Zn: Ti is 16:1. As illustrated in Zn-Ti phase diagram (Figure 3.1), it is proposed that Zn_{16}Ti is the primary intermetallic phase formed in the Zn-0.3 wt% Ti alloy. This result agrees with a previous study that concluded the primary Zn-Ti intermetallic phase was evident in as-cast Zn-Ti

alloys that contained 0.16, 0.18, 0.23, and 0.34 wt% Ti [94]. The amount of the eutectic mixture increased with the Ti content. The SEM micrograph of as-cast Zn-0.3 wt% Ti alloy is presented in Figure 5.7. Similar to the as-cast Zn-0.1 wt% Ti alloy, a lamellar eutectic structure was observed at the boundaries of the as-cast Zn-0.3 wt% Ti alloy. Figure 5.8 presents the X-ray diffraction patterns of as-cast Zn-0.3 wt% Ti alloy. It can be seen that the as-cast Zn-0.3 wt% Ti alloy is mainly composed of the Zn phase and the primary $Zn_{16}Ti$ intermetallic phase. However, the peaks of the $Zn_{16}Ti$ intermetallic phase were very weak. It is possible that only a small amount of $Zn_{16}Ti$ intermetallic phase formed in the as-cast Zn-0.3 wt% Ti alloy.

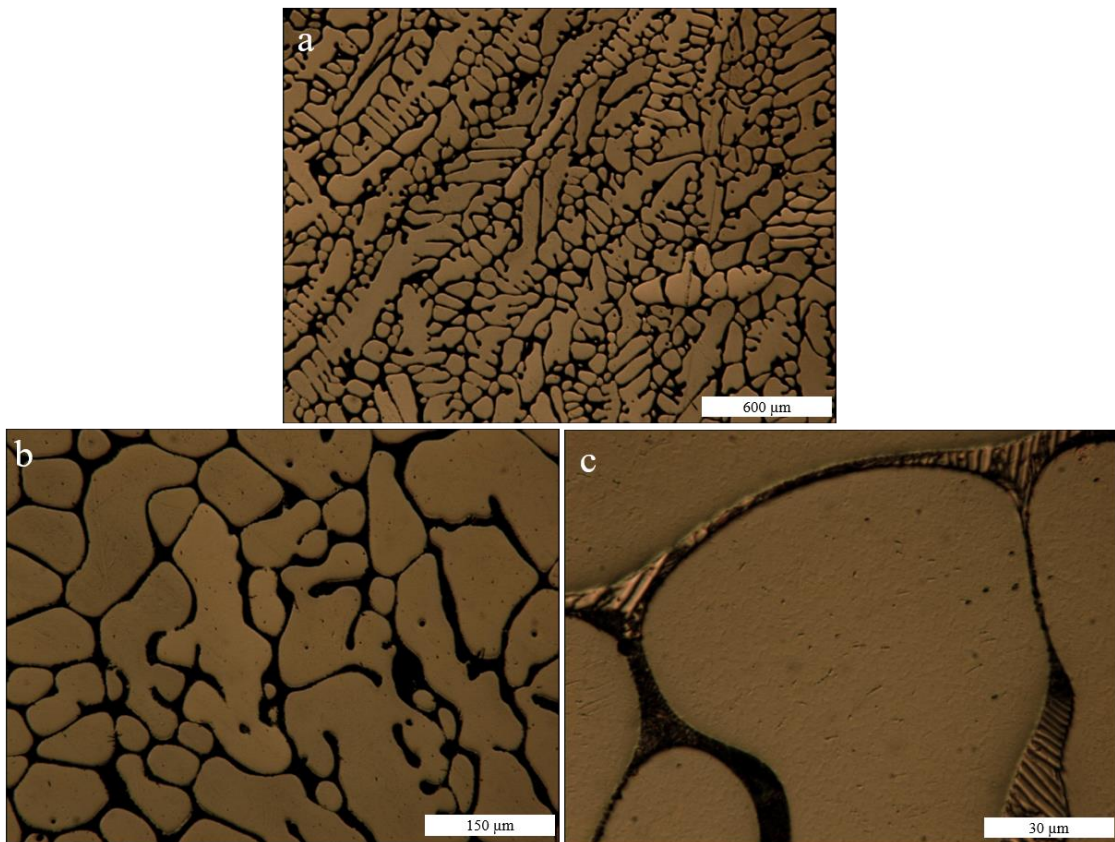


Figure 5.3. Optical micrograph of as-cast Zn-0.1 wt% Ti: a) 25x, b) 100x, c) 500x.

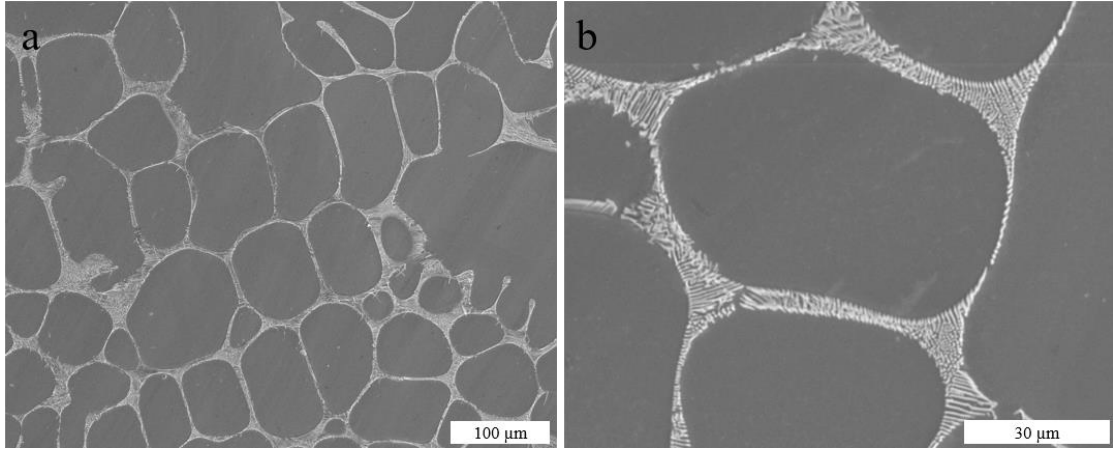


Figure 5.4. SEM micrograph of as-cast Zn-0.1 wt% Ti: a) 200x, b) 1000x.

As shown in Figures 5.1-5.5, the grain size of as-cast Zn-Ti alloys reduces as the Ti content increases from 0.01 wt% to 0.3 wt%. The addition of a small percentage of titanium to zinc leads to a decrease in the grain size of the Zn-Ti alloys. The grain size was reduced from above 600 μm to about 23 μm with the Ti content increasing from 0.01 wt% to 0.3 wt%. Previous studies [95] indicated that the eutectic of zinc and intermetallic phases formed at the boundaries. The eutectic mixture at the boundaries decreased the cast grain size of zinc. For zinc alloys, the addition of a small amount of Ti results in grain refinement [87]. It is proposed that this refinement is due to the formation of the eutectic of zinc and intermetallic phases at the primary grain boundaries. The area fraction of the eutectic mixture increased with the Ti content increasing from 0.01 wt% to 0.3 wt%.

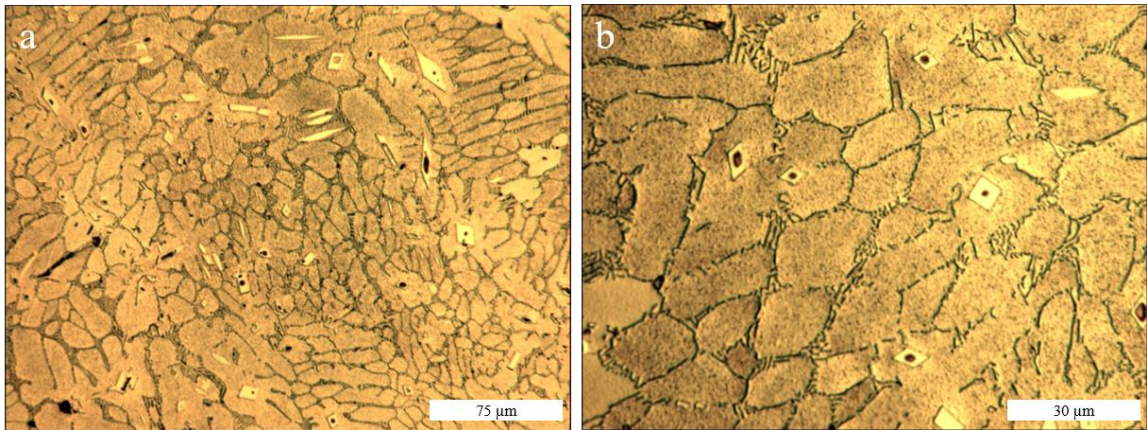


Figure 5.5. Optical micrograph of as-cast Zn-0.3 wt% Ti: a) 200x, b) 500x.

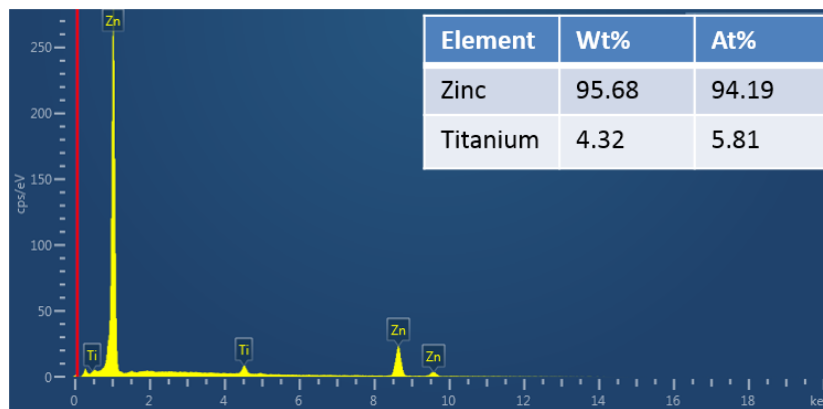


Figure 5.6. EDS point scan of intermetallic phase of as-cast Zn-0.3 wt% Ti alloy.

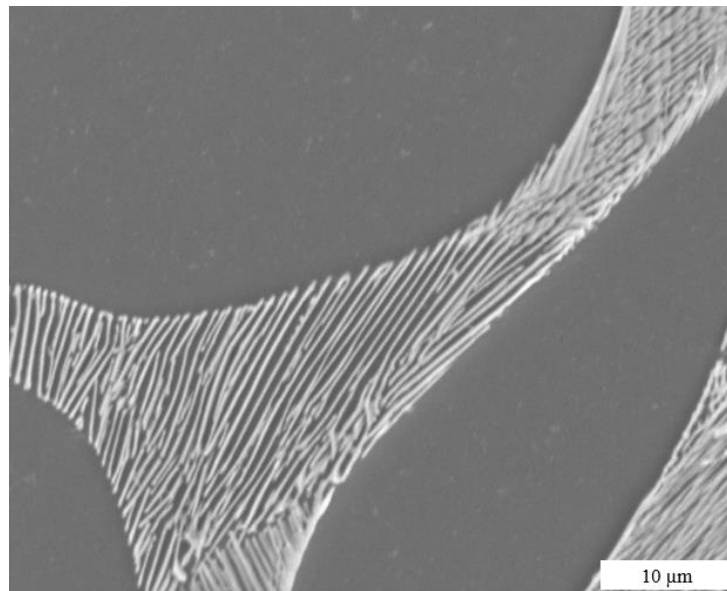


Figure 5.7. SEM micrograph of as-cast Zn-0.3 wt% Ti.

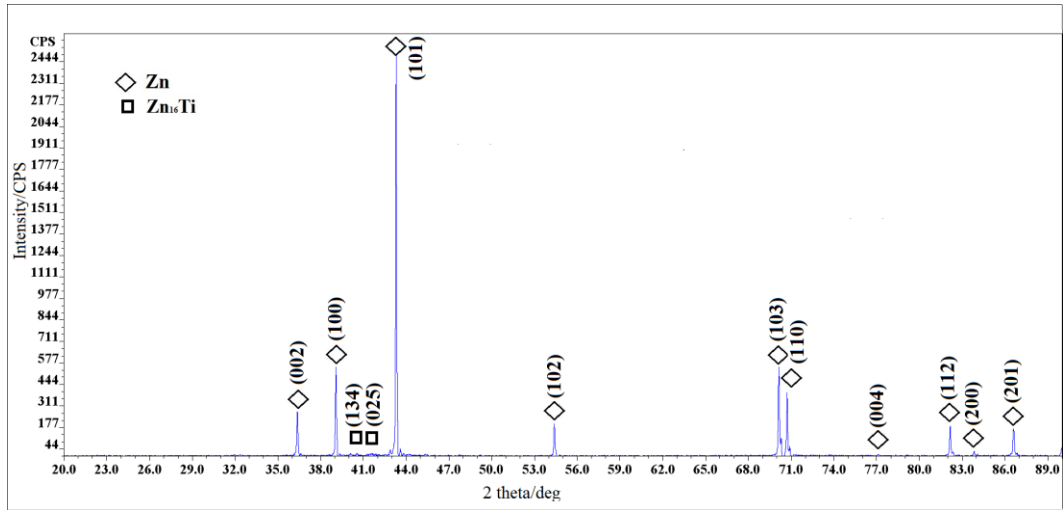


Figure 5.8. X-ray diffraction patterns of as-cast Zn-0.3 wt% Ti alloy.

Zn-0.5 wt% Ti: The optical micrograph of as-cast Zn-0.5 wt% Ti alloy sample is presented in Figure 5.9. Similar to the as-cast Zn-0.3 wt% Ti alloy, primary Zn-Ti intermetallic phases were observed in the as-cast Zn-0.5 wt% Ti alloy. As illustrated in the Zn-Ti phase diagram (Figure 3.1), the Zn-0.5 wt% Ti alloy is hypereutectic. It is proposed that $Zn_{16}Ti$ is the primary intermetallic phase formed in the as-cast Zn-0.5 wt% Ti alloy.

Figure 5.10 shows an SEM micrograph of the as-cast Zn-0.5 wt% Ti alloy. A lamellar eutectic structure was observed in the as-cast Zn-0.5 wt% Ti alloy. The primary Zn-Ti intermetallic phase was found to have a faceted dendritic structure. As illustrated in Figures 5.5 and 5.9, the shape of the primary intermetallic phase changed from faceted to faceted dendritic with the Ti content increasing from 0.3 wt% to 0.5 wt%. Spittle et al. also identified a faceted dendritic primary Zn-Ti intermetallic phase in hypereutectic Zn-Ti alloys [94]. For the as-cast Zn-0.5 wt% Ti alloy, the lamellar eutectic structure became discontinuous as compared to that of as-cast Zn-0.3 wt% Ti alloy. A greater number and

increased size of primary intermetallic phases formed with increasing concentrations of the Ti in the alloy.

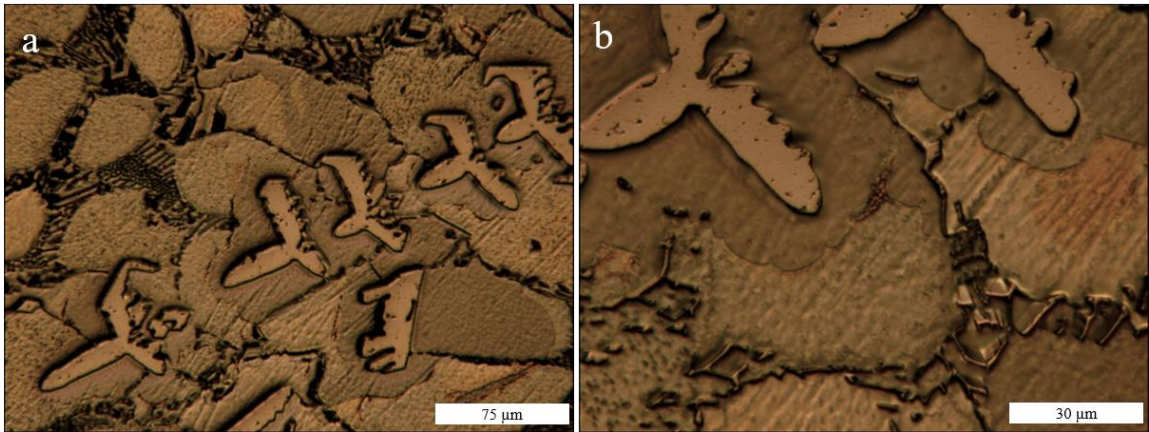


Figure 5.9. Optical micrograph of as-cast Zn-0.5 wt% Ti: a) 200x, b) 500x.

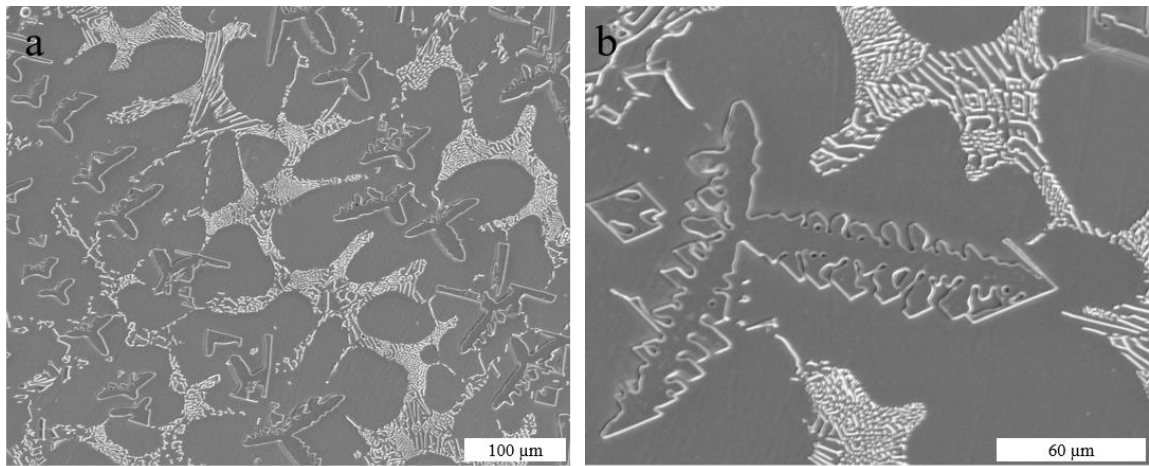


Figure 5.10. SEM micrograph of as-cast Zn-0.5 wt% Ti: a) 200x, b) 500x.

Zn-1 wt% Ti: Similar to the as-cast Zn-0.5 wt% Ti alloy, primary intermetallic phases were formed in the as-cast Zn-1 wt% Ti alloy (Figure 5.11). The area fraction of the intermetallic phase increased as the Ti content increased from 0.3 wt% to 1 wt%. EDS point scans are presented in Figure 5.12 for the as-cast Zn-1 wt% Ti alloy. The EDS

analysis indicated that Zn-Ti intermetallic phases were formed in the as-cast Zn-1 wt% Ti alloy.

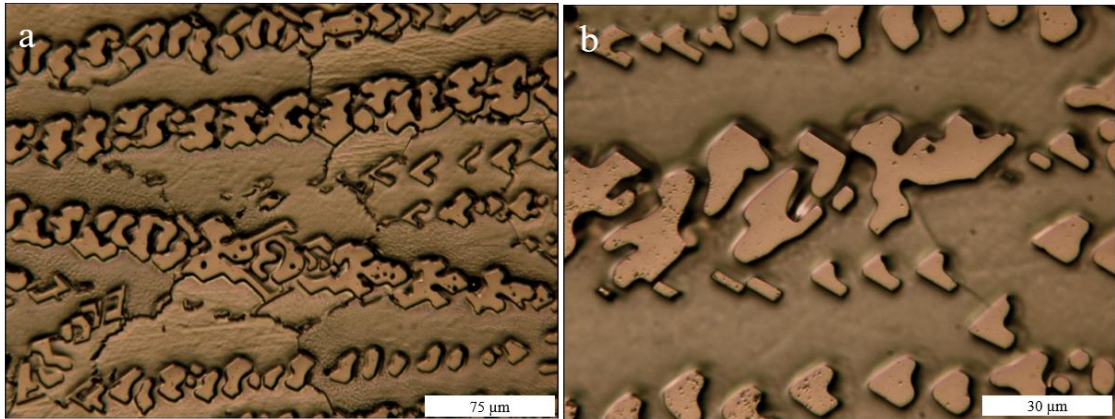


Figure 5.11. Optical micrograph of as-cast Zn-1 wt% Ti: a) 200x, b) 500x.

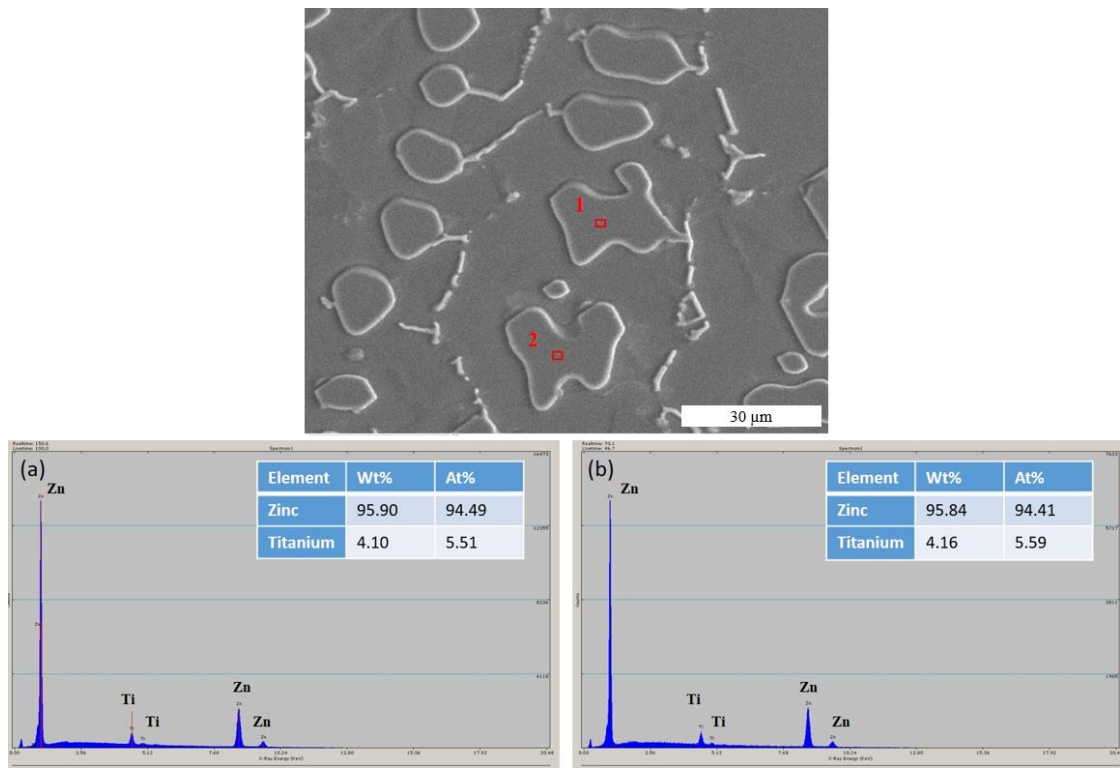


Figure 5.12. EDS point scans of as-cast Zn-1 wt% Ti alloy: a) EDS spectrum of point 1, b) EDS spectrum of point 2.

The Zn-Ti intermetallic phase is approximately 96 wt% Zn and 4 wt% Ti, which is approximately 94 mol% Zn and 6 mol% Ti (Figure 5.12). EDS point scan analysis determined that the approximate mole ratio for Zn: Ti is 16:1. Based on the Zn-Ti phase diagram (Figure 3.1), it is predicted that the final phases of studied Zn-Ti alloys are zinc phase and $Zn_{16}Ti$ intermetallic phase.

Zn-2.5 wt% Ti: The optical micrograph of as-cast Zn-2.5 wt% Ti alloy sample is presented in Figure 5.13. More Zn-Ti intermetallic phases were observed in the as-cast Zn-2.5 wt% Ti alloy compared to the as-cast Zn-1 wt% Ti alloy. It is proposed that increasing the Ti content leads to an increase in the area fraction of the intermetallic phase in this study. Figure 5.14 provides XRD patterns of the as-cast Zn-2.5 wt% Ti alloy. The results indicated the presence of Zn phase and $Zn_{16}Ti$ intermetallic phase. The above results are consistent with the EDS analysis results of the as-cast Zn-1 wt% Ti alloy.

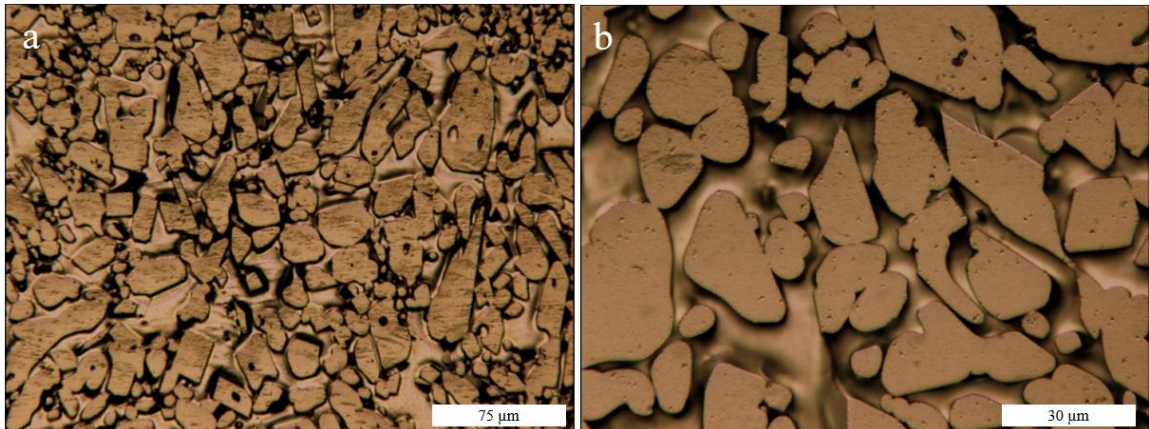


Figure 5.13. Optical micrograph of as-cast Zn-2.5 wt% Ti: a) 200x, b) 500x.

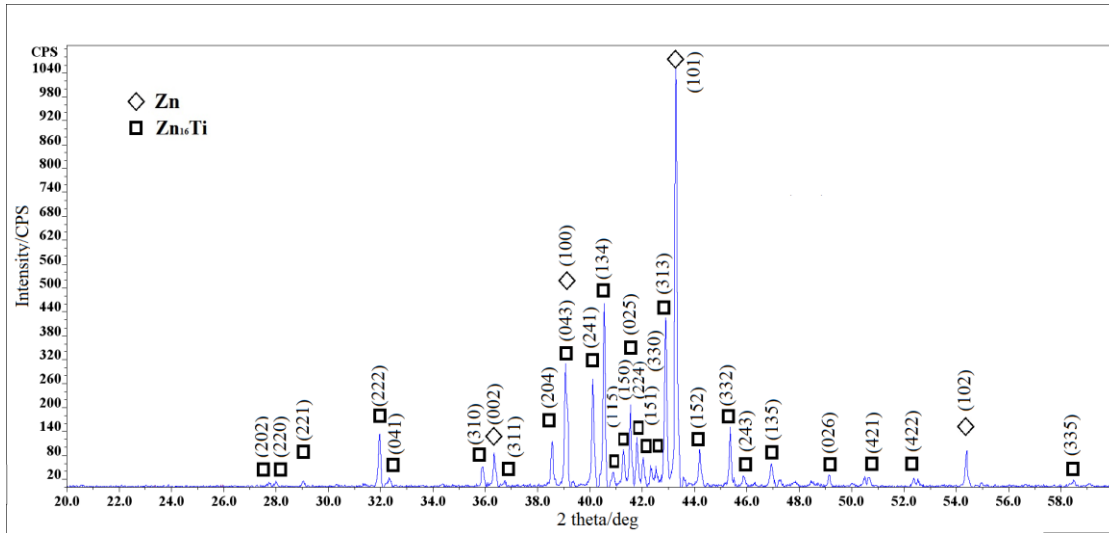


Figure 5.14. X-ray diffraction patterns of as-cast Zn-2.5 wt% Ti alloy.

5.1.2 Hot-extruded Alloys

Zn-0.01 wt% Ti: The optical micrographs of as-extruded Zn-Ti alloys are presented as follows. Figure 5.15 is the optical micrographs of the as-extruded Zn-0.01 wt% Ti alloy. The grain size of as-extruded Zn-0.01 wt% Ti alloy (~14 μm) is markedly smaller than that of as-cast Zn-0.01 wt% Ti alloy (above 600 μm). The near equiaxed grains were observed in the as-extruded macrostructure.

Figure 5.16 shows the SEM micrograph of the as-extruded Zn-0.01 wt% Ti alloy. Zn rich precipitates were uniformly distributed at the grain boundary. As illustrated in the Zn-Ti phase diagram (Figure 3.1), it is proposed that the precipitate formed at the grain boundary is Zn_{16}Ti . Ti was not observed in the precipitates by SEM/EDS because the solubility of Ti in Zn is lower than 0.07 wt% at 300 $^{\circ}\text{C}$. It was very difficult to accurately analyze the Zn rich precipitates within the resolution of SEM/EDS analysis. Figure 5.17 shows the X-ray diffraction patterns of the as-extruded Zn-0.01 wt% Ti alloy. The

analysis of the peaks indicated the presence of a Zn phase in the as-extruded Zn-0.01 wt% Ti alloy.

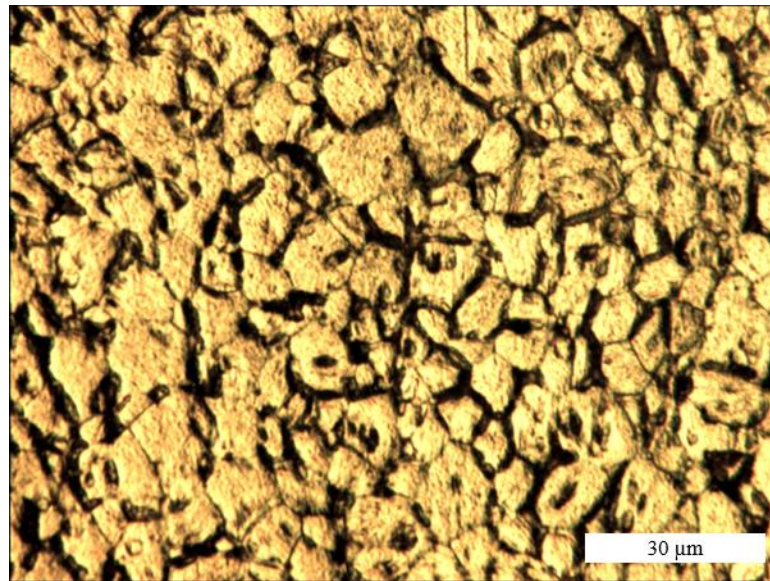


Figure 5.15. Optical micrograph of as-extruded Zn-0.01 wt% Ti.

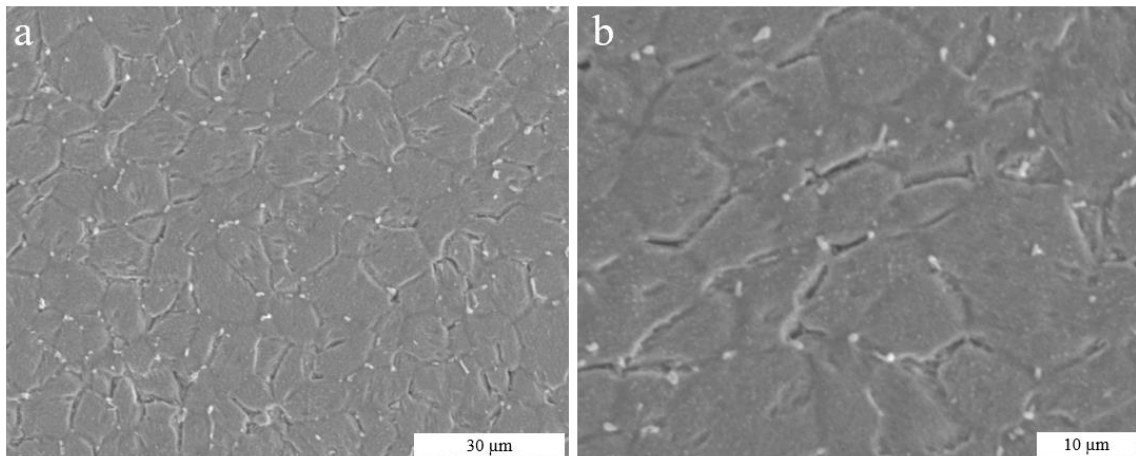


Figure 5.16. SEM micrograph of as-extruded Zn-0.01 wt% Ti: a) 1000x, b) 2000x.

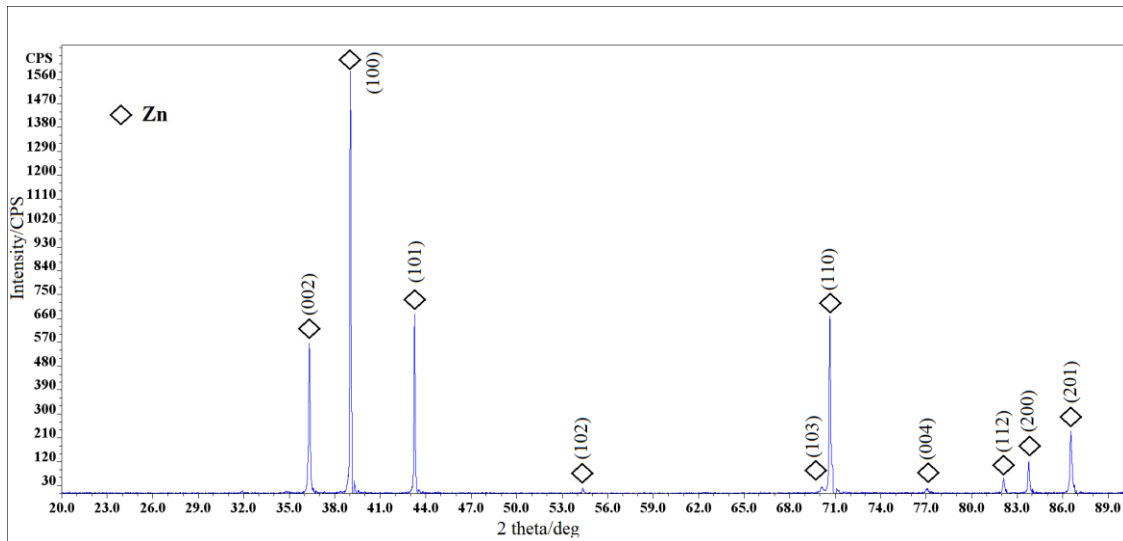


Figure 5.17. X-ray diffraction patterns of as-extruded Zn-0.01 wt% Ti alloy.

Zn-0.1 wt% Ti: Figure 5.18 is the optical micrograph of as-extruded Zn-0.1 wt% Ti alloy sample. As shown in Figures 5.18, it can be seen that as-extruded Zn-0.1 wt% Ti has fine grains when compared with the as-cast Zn-0.1 wt% Ti alloys. Similar to Zn-0.01 wt% Ti alloy, grain refinement of Zn-0.1 wt% Ti alloy was also observed after hot extrusion.

Figure 5.19 is the SEM micrograph of as-extruded Zn-0.1 wt% Ti alloy. It is proposed that the microstructure of as-extruded Zn-0.1 wt% Ti alloy consisted of primary Zn grains and eutectic phases at the boundaries. For the Zn-0.1 wt% Ti alloy, hot extrusion leads to a change in microstructure from dendritic to near equiaxed structures. During hot extrusion processing, large primary Zn dendrite grains disappear and small equiaxial grains form when recrystallization occurs. This result agrees with a previous study that showed that the grain refinement in Zn-1 wt% Mg alloy after hot extrusion transforms large dendritic grains into small equiaxed grains [96].

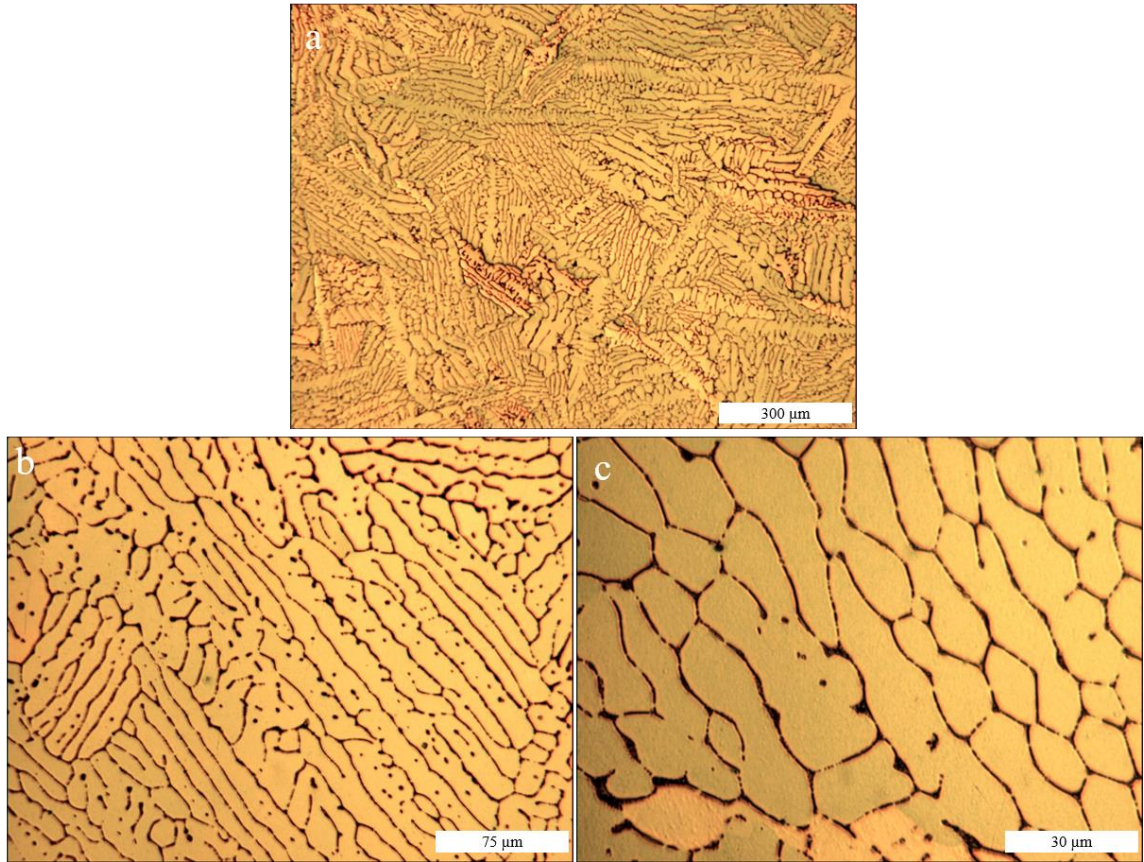


Figure 5.18. Optical micrograph of as-extruded Zn-0.1 wt% Ti: a) 50x, b) 200x, and c) 500x.

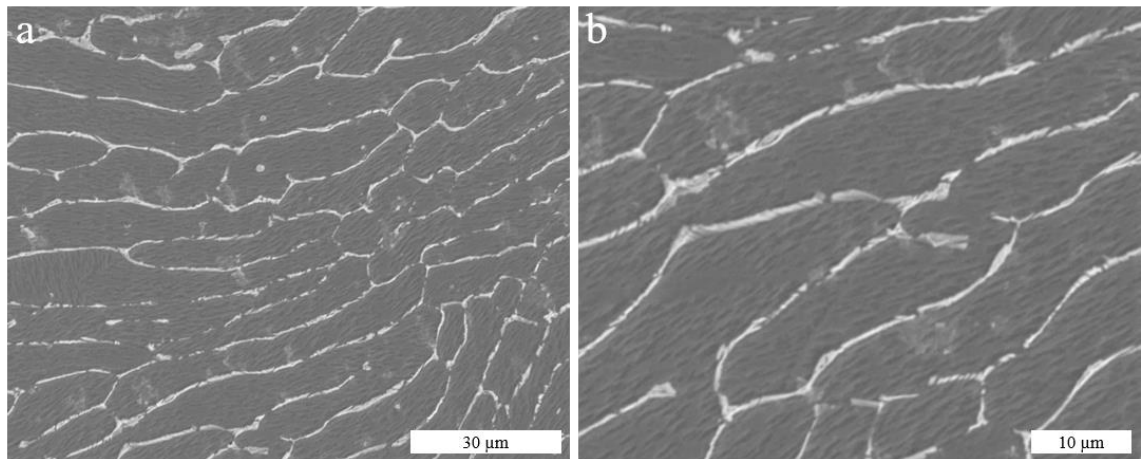


Figure 5.19. SEM micrograph of as-extruded Zn-0.1 wt% Ti: a) 1000x, b) 2000x.

Zn-0.3 wt% Ti: Figure 5.20 is the optical micrographs of the as-extruded Zn-0.3 wt% Ti alloy. Figure 5.21 is the SEM micrograph of as-extruded Zn-0.3 wt% Ti alloy. Similar to the as-cast Zn-0.3 wt% Ti alloy, Zn grains and a eutectic of Zn and intermetallic phase mixtures were observed for the as-extruded Zn-0.3 wt% Ti. Primary Zn-Ti intermetallic phases were also observed in the as-extruded Zn-0.3 wt% Ti alloy. Those precipitates had a faceted structure. For the as-extruded Zn-0.3 wt% Ti, the microstructure is similar for the as-cast Zn-0.3 wt% Ti. The as-cast Zn-0.3 wt% Ti alloy exhibited smaller grains when compared with the as-cast Zn-0.01 wt% Ti and Zn-0.1 wt% Ti alloys. It is predicted that the reduction in grain size of as-cast Zn-0.3 wt% Ti alloy was limited by the hot extrusion process because of fast grain growth at low temperature after recrystallization process.

The X-ray diffraction patterns of as-extruded Zn-0.3 wt% Ti alloy is illustrated in Figure 5.22. Similar to the as-cast Zn-0.3 wt% Ti alloy, the phase of Zn and primary Zn₁₆Ti intermetallic phase were detected in as-extruded Zn-0.3 wt% Ti alloy. The peaks of Zn₁₆Ti intermetallic phase were also very weak.

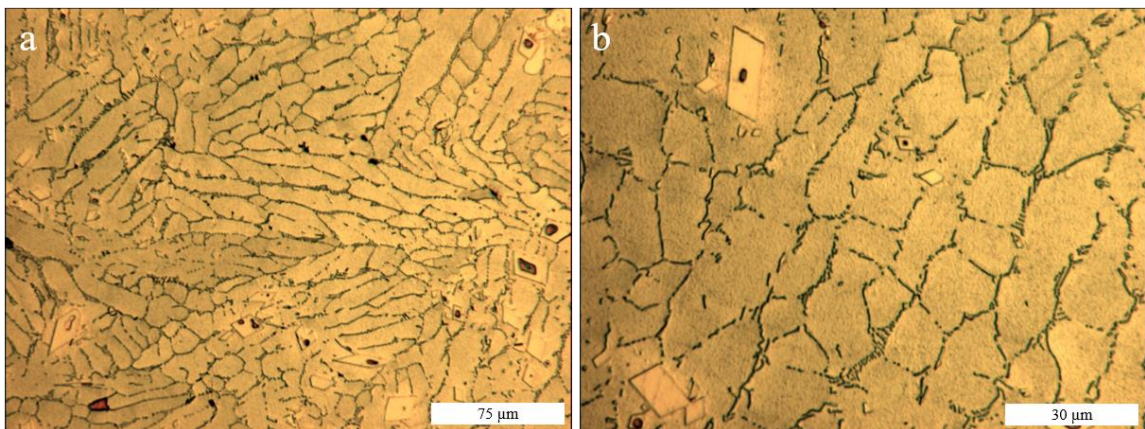


Figure 5.20. Optical micrograph of as-extruded Zn-0.3 wt% Ti: a) 200x, b) 500x.

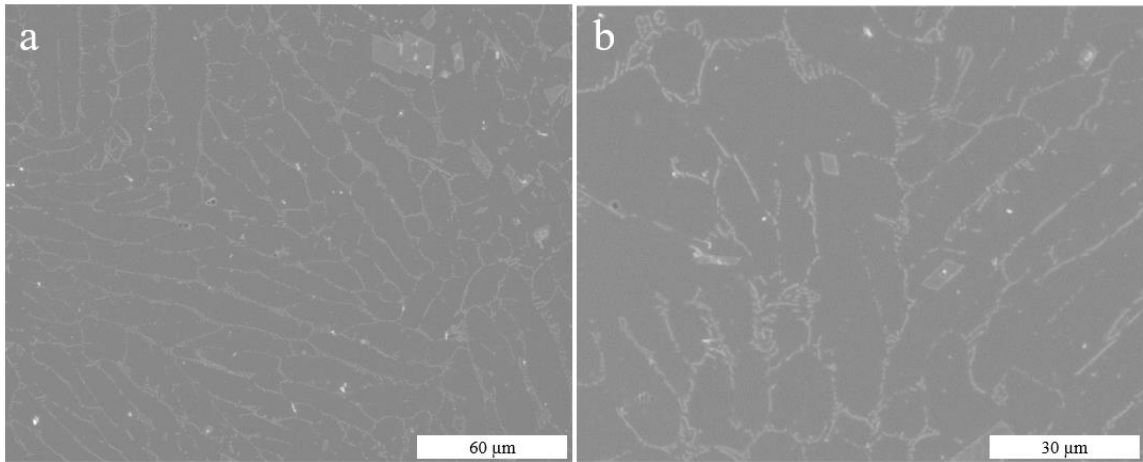


Figure 5.21. SEM micrograph of as-extruded Zn-0.3 wt% Ti: a) 500x, b) 1000x.

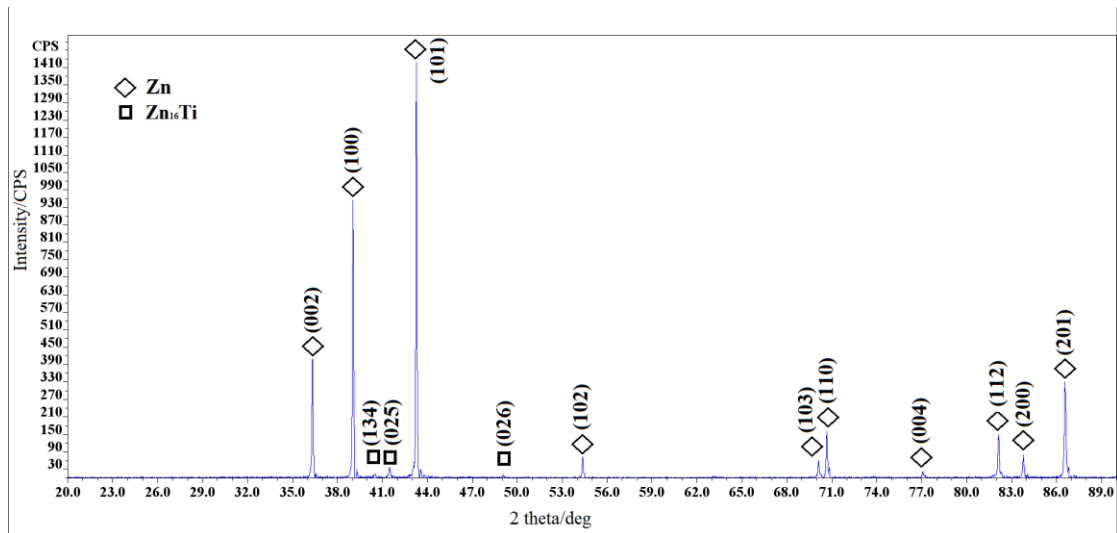


Figure 5.22. X-ray diffraction patterns of as-extruded Zn-0.3 wt% Ti alloy.

5.2 Microhardness

5.2.1 As-cast Alloys

The hardness test results of the as-cast Zn-Ti alloy samples are listed in Table 5.1. A total of 10 indentations were tested at each condition and the error bars represent the standard

deviation for the 10 repeat measurements. The average hardness values were 38, 44, 53, 51, 65, and 99 HV for the six as-cast Zn-Ti alloy conditions. The average hardness for the six different alloys are plotted in Figure 5.23. The as-cast Zn-2.5 wt% Ti had the highest average hardness of 99 HV. The average hardness for as-cast Zn-Ti alloy increased from 38 HV to 99 HV with the Ti content increasing from 0.01 to 2.5 wt%. With increasing Ti content from 0.01 to 0.3 wt%, the average hardness of the as-cast Zn-Ti alloys increased from 38 HV to 53 HV. For as-cast Zn-0.3 wt% Ti, the average hardness values increased by 39% as compared to that of as-cast Zn-0.01 wt% Ti alloy.

As illustrated in the micrographs of the as-cast Zn-Ti alloys (Figures 5.1-5.5), the grain size was reduced with the Ti content increasing from 0.01 to 0.3 wt%. It is proposed that the average hardness of the alloys was increased by the addition of a small amount of Ti, which results in grain refinement. It has been shown that this refinement is due to the formation of a eutectic of zinc and intermetallic phases at the grain boundaries [87].

Table 5.1. Hardness test results of the as-cast Zn-Ti alloys.

Alloy	Average Hardness (HV)	Standard Deviation (HV)
Zn-0.01 wt% Ti	38	2
Zn-0.1 wt% Ti	44	3
Zn-0.3 wt% Ti	53	5
Zn-0.5 wt% Ti	51	3
Zn-1 wt% Ti	65	7
Zn-2.5 wt% Ti	99	10

The average hardness of the as-cast Zn-Ti alloys initially decreased and then increased with the Ti content increasing from 0.3 to 2.5 wt%. The average hardness for the alloys decreased from 53 to 51 HV with the Ti content increasing from 0.3 to 0.5 wt%. The difference between the average hardness values is 2 HV, which was relatively small.

Intermetallic phases were formed in the as-cast Zn-0.5 wt% Ti alloy. It is proposed that the main strengthening mechanism in as-cast Zn-0.5 wt% Ti alloy is the formation of Zn-Ti intermetallic phases. It is predicted that the average hardness of the as-cast Zn-0.5 wt% Ti alloys decreased as compared to that of as-cast Zn-0.3 wt% Ti alloy because the amount of Zn-Ti intermetallic phases formed was quite small. With increasing Ti content from 0.5 to 2.5 wt%, the average hardness of the as-cast Zn-Ti alloys increased. For as-cast Zn-2.5 wt% Ti alloy, the average hardness values increased by 94% as compared to that of as-cast Zn-0.5 wt% Ti alloy.

Increasing Ti content from 0.5 to 2.5 wt% caused the formation of a large amount of Zn-Ti intermetallic phases (Figures 5.9-5.13). It is proposed that the average hardness of the Zn-Ti alloys increased with the Ti content increasing from 0.5 to 2.5 wt% because of the Zn-Ti intermetallic phases.

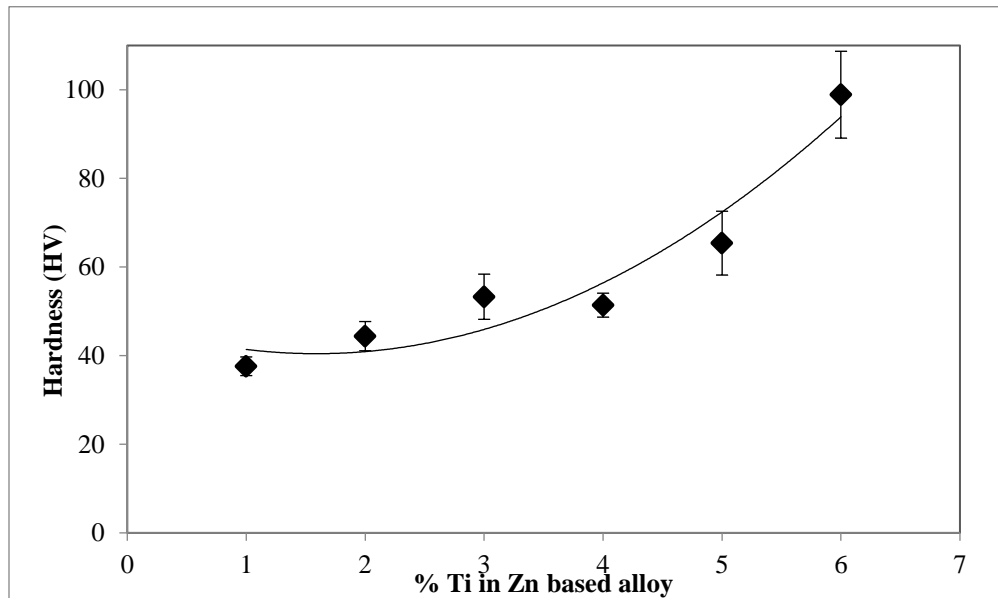


Figure 5.23. The average hardness for the as-cast Zn-Ti alloys.

5.2.2 Hot-extruded Alloys

Table 5.2 lists the hardness test results of the as-extruded Zn-Ti alloy samples. The average hardness values were 72, 60, and 54 HV for the three as-extruded Zn-Ti alloy conditions. The average hardness for the three different alloys are plotted in Figure 5.24.

The as-extruded Zn-0.01 wt% Ti had the highest average hardness of 72 HV. The average hardness for as-extruded Zn-0.01 wt% Ti alloy (72 HV) increased by 89% as compared to that of as-cast Zn-0.01 wt% Ti alloy (38 HV).

As illustrated in Figures 5.1 and 5.15, the grain size of as-extruded Zn-0.01 wt% Ti alloy (~14 μm) is markedly reduced as compared to that of as-cast Zn-0.01 wt% Ti alloy (above 600 μm). SEM/EDS analysis revealed that Zn rich precipitates were observed at the grain boundary for the as-extruded Zn-0.01 wt% Ti alloy. It is predicted that the average hardness of the Zn-0.01 wt% Ti alloys was increased by the hot extrusion process, which results in grain refinement and precipitation.

Table 5.2. Hardness test results of the as-extruded Zn-Ti alloys.

Alloy	Average Hardness (HV)	Standard Deviation (HV)
Zn-0.01 wt% Ti	72	2
Zn-0.1 wt% Ti	60	4
Zn-0.3 wt% Ti	54	2

Similar to the as-extruded Zn-0.01 wt% Ti alloy, the average hardness for as-extruded Zn-0.1 wt% Ti alloy was increased after hot extrusion processing. The average hardness for the as-extruded Zn-0.1 wt% Ti alloy (60 HV) increased by 36% as compared to that of as-cast Zn-0.1 wt% Ti alloy (44 HV). As illustrated in Figure 5.18, small equiaxial grains were observed for the as-extruded Zn-0.1 wt% Ti alloy after hot extrusion. It is

proposed that the average hardness of the as-extruded Zn-0.1 wt% Ti alloys increased because small equiaxial Zn grains formed after hot extrusion.

The average hardness was approximately equal in the extruded and as-cast Zn-0.3 wt% alloy within the reproducibility error. The difference between the average hardness values was 1 HV which was relatively small. From the microstructural point of view, as illustrated in Figures 5.5 and 5.20, it was observed that the grain size of as-extruded and as-cast Zn-0.3 wt% Ti alloy was approximately constant during hot extrusion process. No apparent grain refinement was observed for the Zn-0.3 wt% Ti alloy after hot extrusion. In an investigation of Zn-Mg and Zn-Al alloys, Mostaed et al. observed that no apparent improvement of hardness after hot extrusion [55]. It is proposed that the average hardness was approximately equal in the extruded and as-cast Zn-0.3 wt% alloy because no apparent grain refinement was observed after hot extrusion. The standard deviations for three as-extruded sample conditions were relatively small and this correlated with the observation that the samples had uniform microstructure.

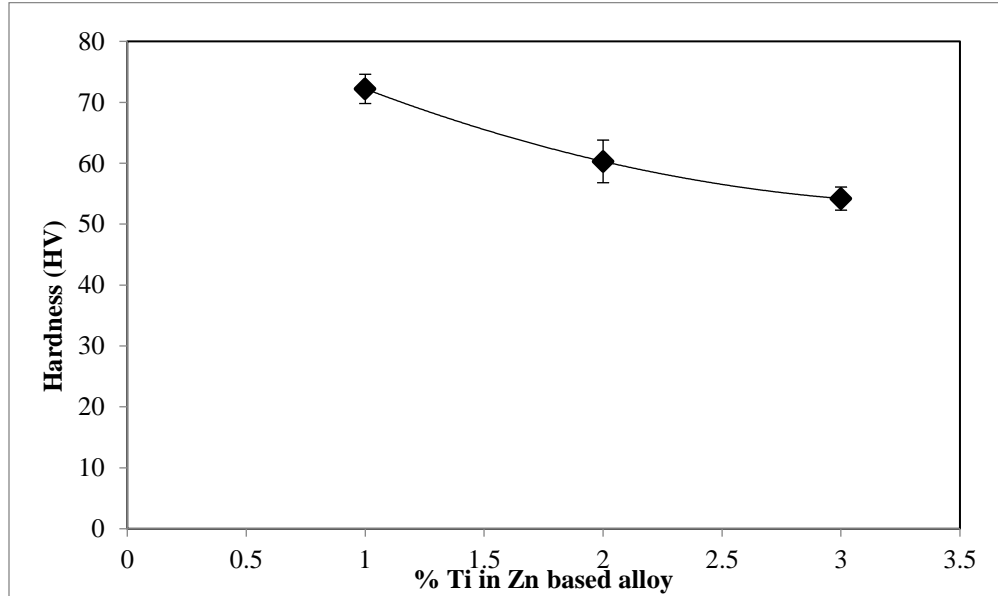


Figure 5.24. The average hardness for the as-extruded Zn-Ti alloys.

5.3 Mechanical Properties

5.3.1 As-cast Alloys

Table 5.3 lists the tensile test results for the five as-cast Zn-Ti alloys. The average ultimate tensile strengths were 101, 115, 141, 150, and 177 MPa for the five as-cast Zn-Ti alloy conditions, respectively. The average ultimate tensile strengths for the five different as-cast alloys are plotted in Figure 5.25. The as-cast Zn-1 wt% Ti had the highest average ultimate tensile strength and yield strength of 177 and 122 MPa, respectively. The average ultimate tensile strength and yield strength for as-cast Zn-Ti alloy increased from 101 and 64 MPa to 177 and 122 MPa, respectively, with the Ti content increasing from 0.01 to 1 wt%. With increasing Ti concentration, both tensile strength and yield strength increased. The above results are consistent with the results of

the hardness test. The standard deviation of five as-cast Zn-Ti alloy sample conditions were relatively small.

The average elongation to failure for the five different as-cast alloys are plotted in Figure 5.26. The average elongation to failure values were 8.5, 12.5, 3.2, 4.3, and 2.3%. The as-cast Zn-0.1 wt% Ti had the highest average elongation to failure of 12.5%. The average elongation to failure of the as-cast Zn-Ti alloys initially increased and then decreased with Ti content increasing from 0.01 to 1 wt%.

Table 5.3. Tensile test results for the as-cast Zn-Ti alloys.

Alloy	Ultimate tensile strength (MPa)	Yield strength (MPa)	Elongation (%)
Zn-0.01 wt% Ti	101±4	64±1	8.5±3.2
Zn-0.1 wt% Ti	115±3	68±2	12.5±4.4
Zn-0.3 wt% Ti	141±5	87±6	3.2±0.3
Zn-0.5 wt% Ti	150±5	81±1	4.3±1.0
Zn-1 wt% Ti	177±7	122±1	2.3±0.3

With increasing Ti content, the ultimate tensile strength and yield strength of the alloys increased (Table 5.3). The ultimate tensile strength of the as-cast Zn-Ti alloys increased from 101 MPa to 141 MPa with the Ti content increasing from 0.01 to 0.3 wt%. For as-cast Zn-0.3 wt% Ti alloy, the average ultimate tensile strengths increased by 40% as compared to that of Zn-0.01 wt% Ti. The as-cast Zn-0.1 wt% Ti alloy reached a highest elongation to failure of 12.5%. The average elongation to failure of the as-cast Zn-Ti alloys initially increased and then decreased with Ti content increasing from 0.01 to 0.3 wt%. From the microstructural point of view, as illustrated in the micrographs of the as-cast Zn-Ti alloys (Figures 5.1-5.5), the grain size for zinc alloy decreased from above 600 μm to about 23 μm with the Ti content increasing from 0.01 wt% to 0.3 wt%. This result

agrees with a previous study that the addition of a small percentage of titanium to zinc resulted in grain refinement because the number of zinc-rich grains increased with increasing the Ti content [84]. It has been shown that this refinement is due to the formation of eutectic of zinc and intermetallic phases at the grain boundaries [87]. Based on the Hall-Petch relation [97], it is proposed that with the Ti content increasing from 0.01 to 0.3 wt%, the strength of as-cast Zn-Ti alloys increased with a decrease in the grain size. The average elongation to failure of the as-cast Zn-0.3 wt% Ti alloy (3.2%) decreased by 74% as compared to that of as-cast Zn-0.1 wt% Ti alloy (12.5%). As illustrated in Figure 5.5, it was observed that primary Zn-Ti intermetallic phases were observed in the as-cast Zn-0.3 wt% Ti alloy. It is proposed that the formation of Zn-Ti intermetallic phases results in lower elongation to failure of the as-cast Zn-0.3 wt% Ti alloy.

The as-cast Zn-1 wt% Ti had the highest average ultimate tensile strength (177 MPa). The ultimate tensile strength of the as-cast Zn-Ti alloys increased from 150 MPa to 177 MPa with the Ti content increasing from 0.5 to 1 wt%. For as-cast Zn-1 wt% Ti alloy, the average ultimate tensile strengths increased by 18% as compared to that of as-cast Zn-0.5 wt% Ti. Zn-Ti intermetallic phases were observed in the Zn-0.5 wt% Ti alloy (Figure 5.9). Increasing Ti content from 0.5 to 1 wt% caused the formation of a large amount of Zn-Ti intermetallic phases (Figures 5.9 and 5.11). The larger Ti content resulted in an increase in the area fraction of Zn-Ti intermetallic phases. The addition of Ti caused strong hardening of alloy with the formation of Zn-Ti intermetallic phase [85, 86]. It is proposed that the average ultimate tensile strength of the as-cast Zn-Ti alloys increased with the Ti content increasing from 0.5 to 1 wt% because of the Orowan strengthening

with Zn-Ti intermetallic phases [98]. The average elongation to failure values of the as-cast Zn-0.5 wt% Ti and Zn-1 wt% Ti alloys did not exceed 5%. This low elongation of the as-cast Zn-0.5 wt% Ti and Zn-1 wt% Ti alloys was attributed to the increasing content of the Zn-Ti intermetallic phases (Figures 5.9 and 5.11).

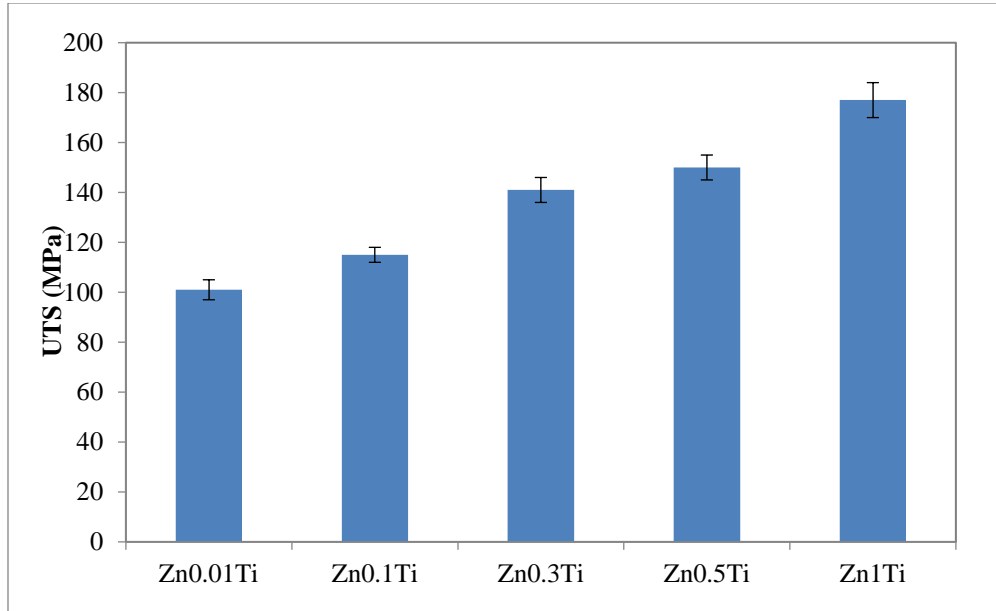


Figure 5.25. The average ultimate tensile strength for the as-cast Zn-Ti alloys.

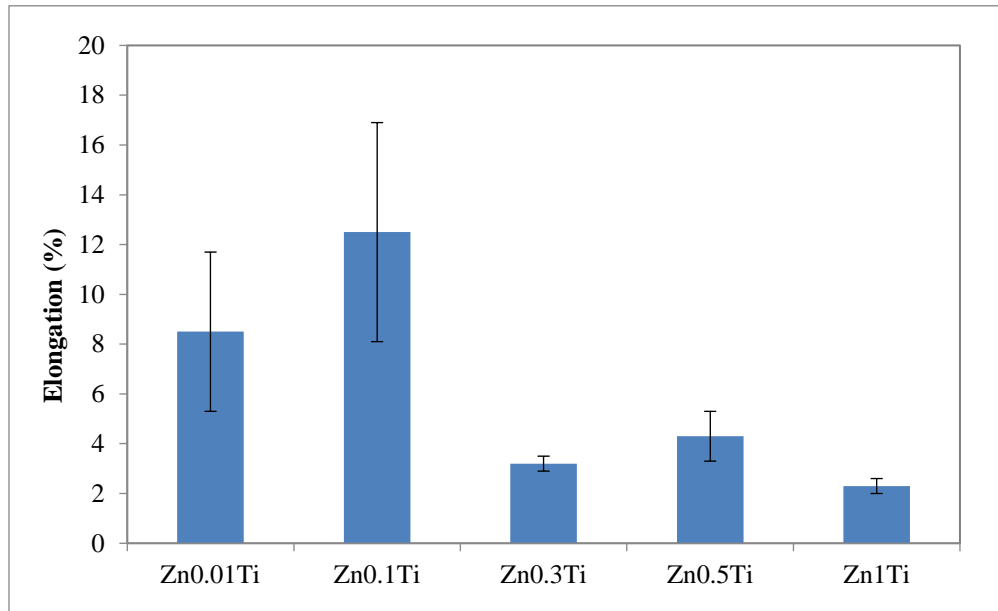


Figure 5.26. The average elongation to failure for the as-cast Zn-Ti alloys.

5.3.2 Hot-extruded Alloys

Table 5.4 lists the tensile test results for the three as-extruded Zn-Ti alloys. The representative stress-strain curve for the three as-extruded Zn-Ti alloys are plotted in Figure 5.27. The average ultimate tensile strengths were 269, 207, and 199 MPa for the three as-extruded Zn-Ti alloys respectively. The average ultimate tensile strengths for the three different alloy conditions are plotted in Figure 5.28. The as-extruded Zn-0.01 wt% Ti had the highest average ultimate tensile strength and yield strength of 269 and 177 MPa. The average ultimate tensile strength and yield strength for as-extruded Zn-Ti alloy decreased from 269 and 177 MPa to 199 and 143 MPa with the Ti content increasing from 0.01 to 0.3 wt%. Based on the homogenization kinetics, the as-cast Zn-Ti ingots were not homogenized well enough before hot extrusion processing. It is possible that a uniform composition throughout the grains was not achieved after homogenization

process contributing to the lower of tensile and yield strength of the as-extruded Zn-Ti alloy with the Ti contents ranging from 0.1 wt% to 0.3 wt%.

The average elongation to failure values for the three different as-extruded alloy conditions are plotted in Figure 5.29. The average elongation to failure values were 11, 44, and 30%, respectively. The as-extruded Zn-0.1 wt% Ti had the highest average elongation to failure of 44%. The average elongation to failure of the as-extruded Zn-Ti alloys initially increased and then decreased with Ti content increasing from 0.01 to 0.3 wt%.

Table 5.4. Tensile test results for the as-extruded Zn-Ti alloys.

Alloy	Ultimate tensile strength (MPa)	Yield strength (MPa)	Elongation (%)
Zn-0.01 wt% Ti	269±5	177±24	10.9±0.4
Zn-0.1 wt% Ti	207±3	163±13	43.8±1.9
Zn-0.3 wt% Ti	199±2	143±6	29.8±1.4

As illustrated in Tables 5.3-5.4, the average ultimate tensile strength, yield strength, and elongation to failure of the three Zn-Ti alloy conditions (Zn-0.01Ti, Zn-0.1Ti, and Zn-0.3Ti) were improved after hot extrusion. Compared with as-cast Zn-0.01 wt% Ti alloy (UTS=101 MPa, YS=64 MPa), the as-extruded Zn-0.01 wt% Ti alloy (UTS=269 MPa, YS=177 MPa) has 166% and 177% improvement in ultimate tensile strength and yield strength, respectively. It is proposed that a remarkable increase in the ultimate tensile strength and yield strength in as-extruded Zn-0.01 wt% Ti alloy is due to grain refinement after hot extrusion processing. As illustrated in Figure 5.16, Zn rich precipitates were observed at the grain boundary for the as-extruded Zn-0.01 wt% Ti alloy. It is likely that natural aging after hot extrusion process leads to formation of the

Zn rich precipitates at the grain boundary. Based on the Zn-Ti phase diagram (Figure 3.1), the solid solubility of titanium in zinc is very limited. The $Zn_{16}Ti$ intermetallic phase forms when the alloying element Ti is at concentrations above its solubility limit. The final phases of studied Zn-0.01 wt% Ti alloy are Zn-rich solid solution phase and eutectic containing Zn and intermetallic phase $Zn_{16}Ti$ at the grain boundary while some intermetallic phase $Zn_{16}Ti$ precipitates inside grains. The intermetallic phase $Zn_{16}Ti$ inside grains continues to precipitate and migrate to grain boundaries over time. The formation of the intermetallic phase $Zn_{16}Ti$ along the grain boundaries over time may results in Zn rich precipitates and the natural aging-hardening. It is also possible that the formation of precipitates at the grain boundary results in higher strength of the as-extruded Zn-0.01 wt% Ti alloy.

The average elongation to failure values were 9% and 11% for as-cast and as-extruded Zn-0.01 wt% alloy samples, respectively. The average elongation was approximately equal in the as as-extruded and as-cast Zn-0.01 wt% alloy within the reproducibility error. It is proposed that the average elongation to failure of as-extruded Zn-0.01 wt% alloy was relatively low because the precipitates at the grain boundary can initiate stress-induced microcracks, which leads to a reduction in the elongation [96]. The standard deviations for as-extruded Zn-0.01 wt% Ti alloy sample condition were relatively small (0.4%) and this correlated with the observation that the samples had uniform microstructure. However, the standard deviation of as-cast Zn-0.01 wt% Ti alloy sample condition was relatively large (3.2%).

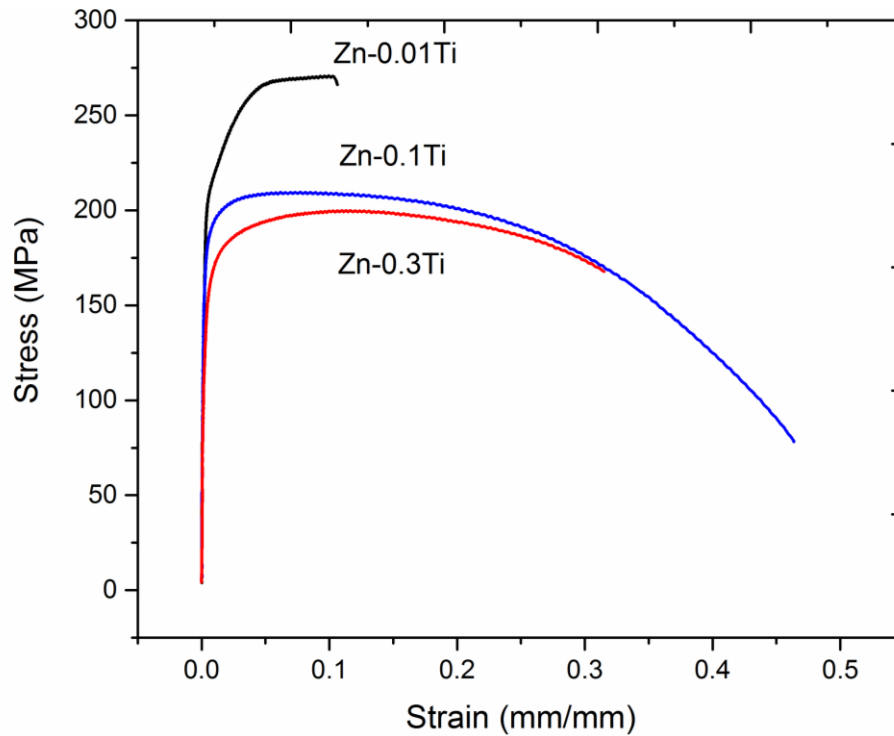


Figure 5.27. Stress-strain curves for the as-extruded Zn-Ti alloys.

Similar to the Zn-0.01 wt% Ti alloy, the ultimate tensile strength and yield strength were improved for Zn-0.1 wt% Ti and Zn-0.3 wt% Ti alloys. Therefore, the thermal deformation is effective in improving the mechanical properties of Zn-Ti alloys. The ultimate tensile strength and yield strength for as-extruded Zn-0.1 wt% Ti alloy (UTS=207 MPa, YS=163 MPa) increased by 80% and 140% as compared to that of as-cast Zn-0.1 wt% Ti alloy (UTS=115 MPa, YS=68 MPa). It was observed that the grain refinement of Zn-0.1 wt% Ti alloy after hot extrusion. As illustrated in Figure 5.18, small equiaxial grains were observed for the as-extruded Zn-0.1 wt% Ti alloy after hot extrusion. It is predicted that the strength of the as-extruded Zn-0.1 wt% Ti alloys increased because the small equiaxial Zn grains formed after hot extrusion process.

Compared with as-cast Zn-0.3 wt% Ti alloy (UTS=141 MPa, YS=87 MPa), the as-extruded Zn-0.3 wt% Ti alloy (UTS=199 MPa, YS=143 MPa) has 41% and 64% improvement for ultimate tensile strength and yield strength, respectively. The increase in strength of as-extruded Zn-0.3 wt% Ti alloy is relatively less significant compared with that of as-extruded Zn-0.1 wt% Ti alloy after hot extrusion process. As illustrated in Figures 5.5 and 5.20, it was observed that the grain size of as-cast and as-extruded Zn-0.3 wt% Ti alloy was approximately the same. No apparent grain refinement was identified for Zn-0.3 wt% Ti alloy after hot extrusion. It is predicted that the reduction in grain size of as-cast Zn-0.3 wt% Ti alloy was limited by the hot extrusion process because of fast grain growth at low temperature after recrystallization. It is also possible that the increase in strength of as-extruded Zn-0.3 wt% Ti alloy is relatively less significant because no apparent grain refinement was observed after hot extrusion process.

The as-extruded Zn-0.1 wt% Ti and Zn-0.3 wt% Ti alloys exhibited excellent ductility, which have high elongation of 44% and 30%, respectively. The elongation to failure for the as-extruded Zn-0.1 wt% Ti alloy condition was relatively large (44%). The elongation of the as-extruded Zn-0.1 wt% Ti alloy (44%) increased by 250% as compared to that of as-cast Zn-0.1 wt% Ti alloy (13%). As illustrated in Figures 5.3 and 5.18, the microstructure of Zn-0.1 wt% Ti alloy could be remarkably modified from coarse primary Zn dendrite grains to small equiaxial grains after hot extrusion. It is proposed that the as-extruded Zn-0.1 wt% Ti alloy exhibited excellent ductility (44%) due to the grain refinement and grain shape adjustment after hot extrusion.

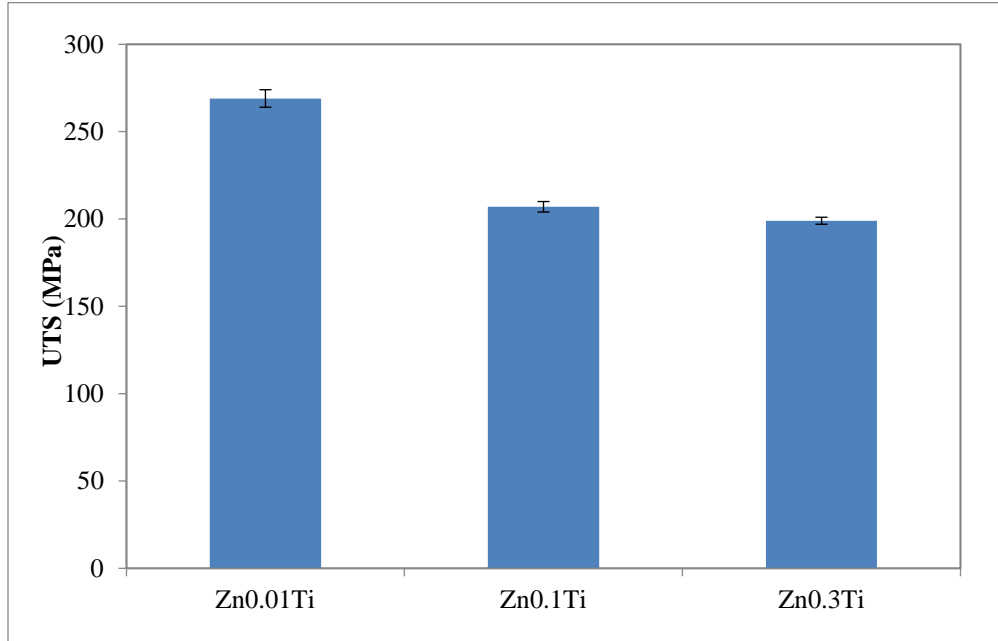


Figure 5.28. The average ultimate tensile strength for the as-extruded Zn-Ti alloys.

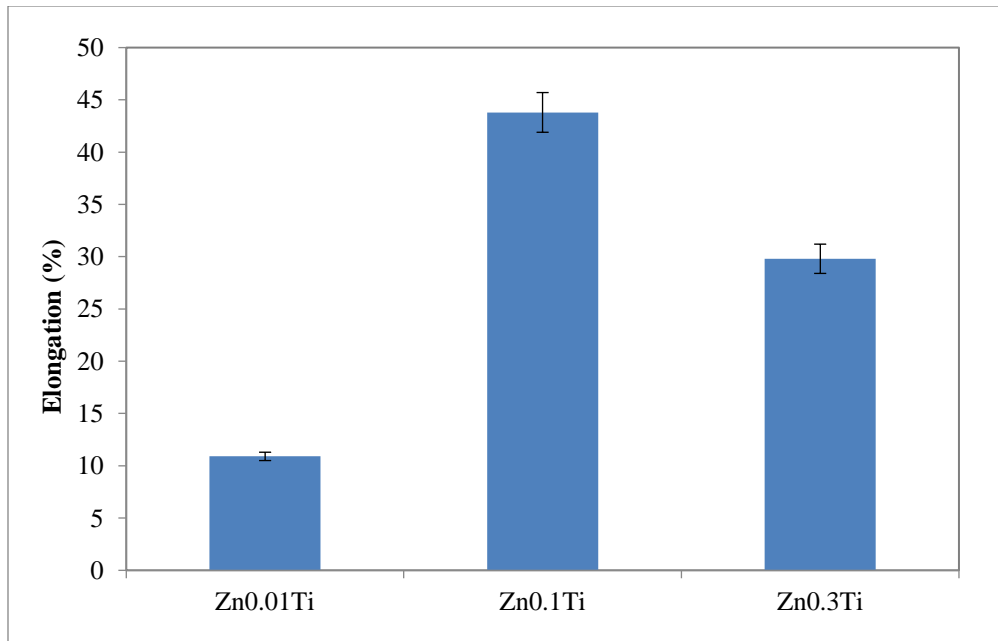


Figure 5.29. The average elongation to failure for the as-extruded Zn-Ti alloys.

5.4 Fractography

The SEM micrographs of as-cast and as-extruded Zn-Ti alloy sample fracture surfaces after tensile tests are presented in Figures 5.30-5.35. Figure 5.30 demonstrates the SEM micrograph of the as-cast Zn-0.01 wt% Ti alloy fracture surface. The as-cast Zn-0.01 wt% Ti alloy exhibited a large number of cleavage planes indicating it was a fracture mode of brittle fracture. It is proposed that the cleavage planes were generated due to the coarse-grained structure of the as-cast Zn-0.01 wt% Ti alloy. The fracture mode of brittle fracture of the as-cast Zn-0.01 wt% Ti alloy is also consistent with its low elongation (9%).

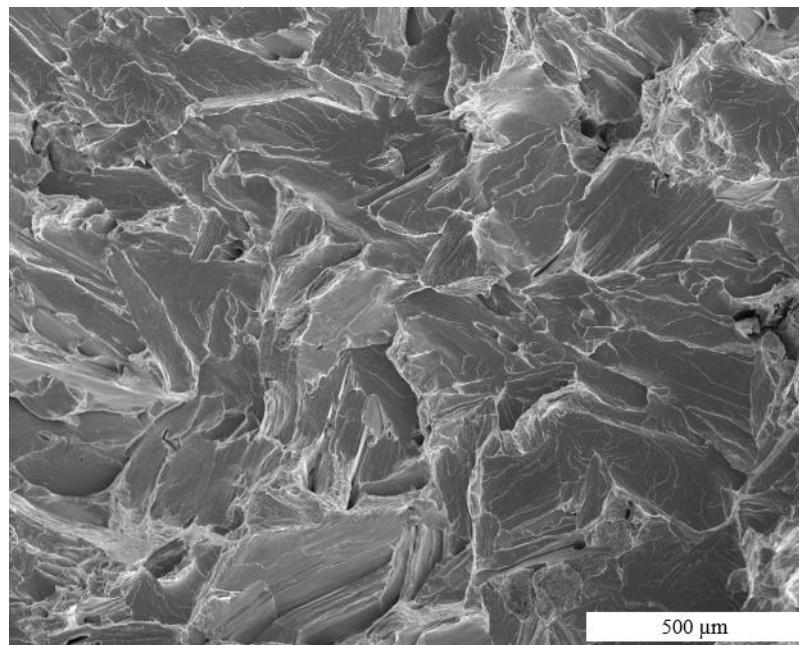


Figure 5.30. SEM micrograph of the fracture surface of as-cast Zn-0.01 wt% Ti.

The SEM micrograph of as-cast Zn-0.1 wt% Ti alloy fracture surface is presented in Figure 5.31. It was observed that almost all the fracture surface of as-cast Zn-0.1 wt% Ti was covered with cleavage planes. It was concluded that the as-cast Zn-0.1 wt% Ti alloy

also exhibited brittle behavior in spite of the fact that it had the highest elongation to failure of 13% of the five as-cast Zn-Ti alloy conditions.

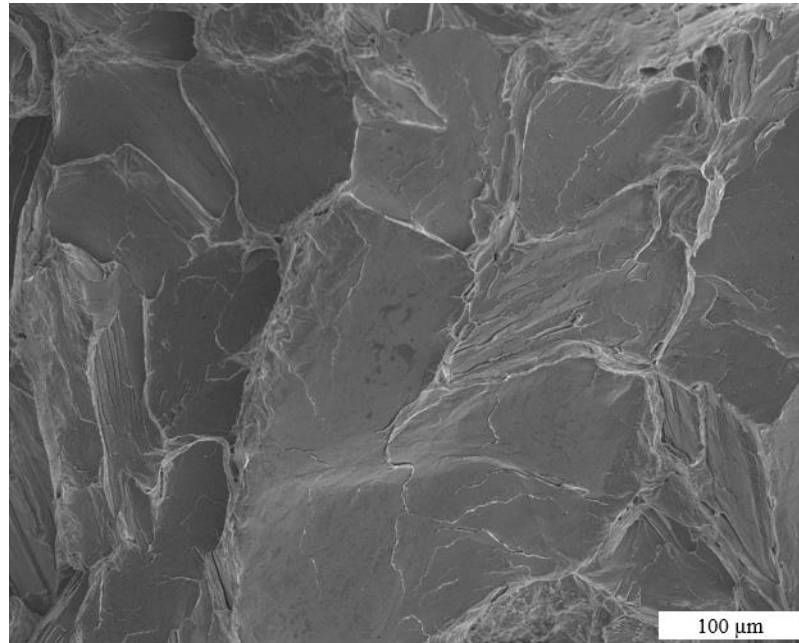


Figure 5.31. SEM micrograph of the fracture surface of as-cast Zn-0.1 wt% Ti.

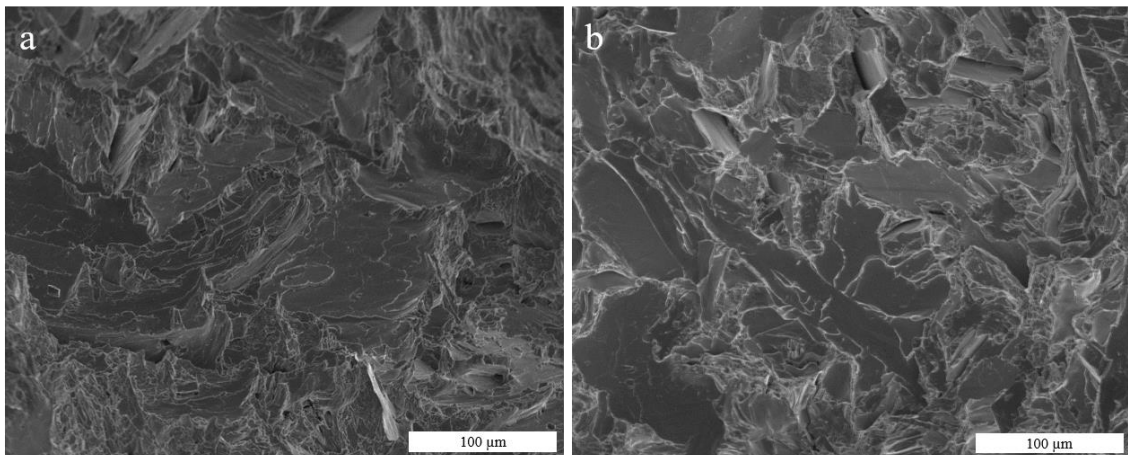


Figure 5.32. SEM micrograph of the fracture surface of as-cast a) Zn-0.3 wt% Ti and b) Zn-1 wt% Ti.

The SEM micrographs of as-cast Zn-0.3 wt% Ti and Zn-1 wt% Ti alloy fracture surface are presented in Figure 5.32. As observed in Figure 5.32, cleavage planes were apparent

on the fracture surface of the as-cast Zn-0.3 wt% Ti and Zn-1 wt% Ti alloy. As illustrated in Figures 5.5 and 5.11, Zn-Ti intermetallic phases were observed in the as-cast Zn-0.3 wt% Ti and Zn-1 wt% Ti alloy which leads to a cleavage fracture mode. With increasing Ti concentration, the number of intermetallic phases increased in this study. The above results are consistent with the results of the tensile test. The average elongation to failure values of the as-cast Zn-0.3 wt% Ti (3%) and Zn-1 wt% Ti (2%) alloy conditions were relatively small.

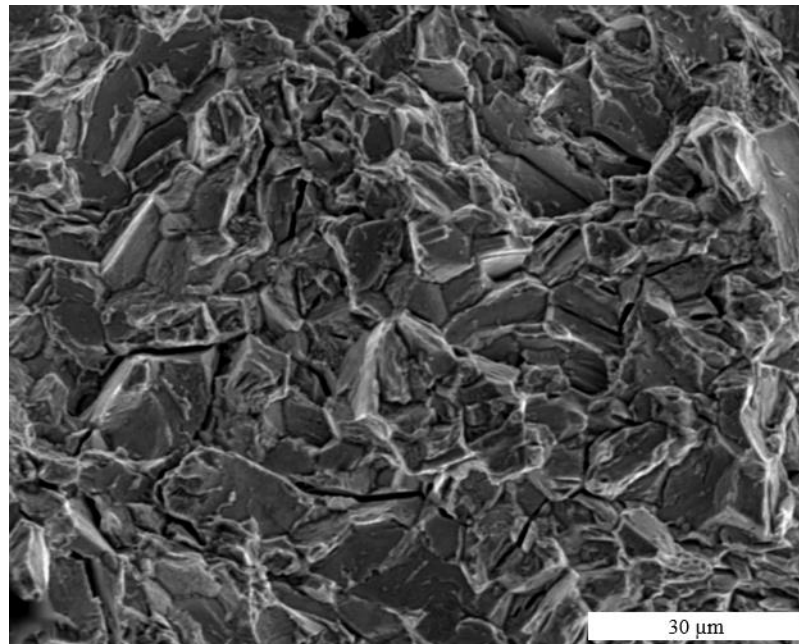


Figure 5.33. SEM micrograph of the fracture surface of as-extruded Zn-0.01 wt% Ti.

Figure 5.33 demonstrates the SEM micrograph of the as-extruded Zn-0.01 wt% Ti alloy fracture surface. Micro-cracks were observed along the grain boundaries of as-extruded Zn-0.01 wt% Ti. It was concluded that the as-extruded Zn-0.01 wt% Ti alloy exhibited intergranular fracture mode. As illustrated in Figure 5.16, it can be seen that Zn rich precipitates were uniformly distributed at the grain boundary. It is predicted that the

micro-cracks were generated due to the precipitates located along grain boundaries of the as-extruded Zn-0.01 wt% Ti alloy. It was also observed that flat fracture facets were apparent on the fracture surface of the as-extruded Zn-0.01 wt% Ti alloy.

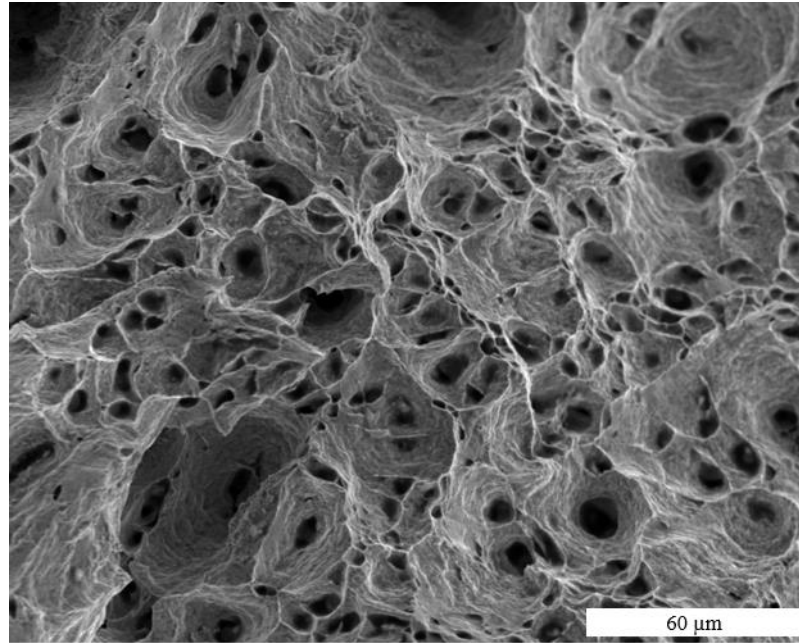


Figure 5.34. SEM micrograph of the fracture surface of as-extruded Zn-0.1 wt% Ti.

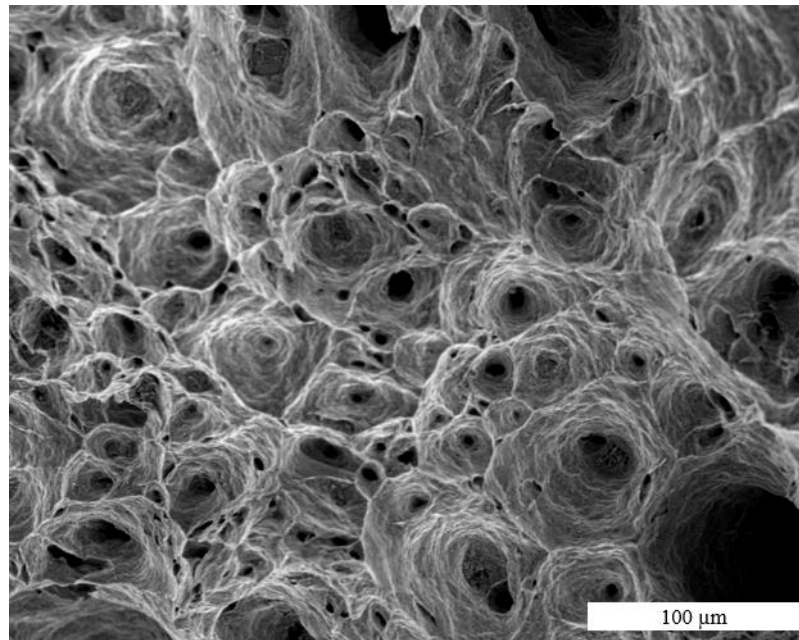


Figure 5.35. SEM micrograph of the fracture surface of as-extruded Zn-0.3 wt% Ti.

Figures 5.34 and 5.35 demonstrate the SEM micrograph of the as-extruded Zn-0.1 wt% Ti and Zn-0.3 wt% Ti alloy fracture surface. For the as-extruded Zn-0.1 wt% Ti alloy, large numbers of dimples were observed on the fracture surface, indicating it was a ductile fracture mode. The ductile fracture mode of the as-extruded Zn-0.1 wt% Ti alloy is consistent with its high elongation (44%). It is predicted that the as-extruded Zn-0.1 wt% Ti alloy exhibited ductile fracture mode due to the grain refinement and homogenization after hot extrusion. Similar to the as-extruded Zn-0.1 wt% Ti alloy, many dimples were also observed on the fracture surface for the as-extruded Zn-0.3 wt% Ti alloy indicating a ductile fracture mode.

6 Conclusions

A series of Zn-Ti alloys with the Ti content of less than 3 wt% was fabricated by vacuum induction melting and processed using a hot extrusion. Mechanical properties of the Zn-Ti alloys were evaluated for endovascular stenting applications. The following are major conclusion reached in this study:

- (1) The as-cast Zn-Ti alloys with Ti content from 0.01 wt% to 2.5 wt% fail to achieve the benchmark the tensile strength of at least 200 MPa (preferably close to 300 MPa) and an elongation to failure of at least 15% (preferably above 20%) required for stenting applications. However, after hot extrusion, the benchmark values were nearly achieved for the Zn-0.1 wt% Ti alloy (UTS=207 MPa, YS=163 MPa, and Elongation=44%). Further improvement through an adjustment of alloy composition or its processing is needed to increase the strength of this alloy above 200 MPa without compromising elongation to failure to less than 30%.
- (2) Extrusion of Zn-Ti microalloys (Zn-0.01Ti, Zn-0.1Ti, and Zn-0.3Ti) at 250 °C with an extrusion ratio of 9:1 concluded with grain refinement. Specifically, large primary Zn dendrite grains disappeared and small nearly equiaxed grains formed when recrystallization occurred after extrusion. Zn rich intermetallic precipitates were also observed at the grain boundaries after extrusion. As a result of grain refinement the tensile strength increased from over 160% to about 80% for Zn-0.01Ti and Zn-0.1Ti microalloys, respectively.
- (3) The as-extruded Zn-0.1 wt% Ti and Zn-0.3 wt% Ti alloys exhibited exceptionally high ductility with elongation to failure of 44% and 30%, respectively. These ductility

values are likely a result of grain refinement and grain shape adjustment caused by extrusion. The high elongation to failure values are consistent with a ductile fracture observed for these alloys.

(4) Both the hardness and strength of the as-cast Zn-Ti alloys increased with increasing Ti content from 0.01 wt% to 2.5 wt%. The grain size was reduced from above 600 μm to $\sim 23 \mu\text{m}$ with the Ti content increasing from 0.01 wt% to 0.3 wt%, and remained only slightly affected for alloys with higher Ti content. Therefore, only a small percentage of Ti was needed to refine grains of Zn. This effect is attributed to low solubility of Ti in Zn and formation of the intermetallic phase. It is proposed that the hardness and strength of the as-cast Zn-Ti alloys increased with the Ti content increasing from 0.3 to 2.5 wt% because the formation of a large amount of Zn-Ti intermetallic phases.

(5) Higher alloying element Ti caused more Zn_{16}Ti intermetallic phases. It is proposed that the formation of Zn-Ti intermetallic phases results in lower elongation to failure of the as-cast Zn-0.3 wt% Ti (3%), Zn-0.5 wt% Ti (4%), and Zn-1 wt% Ti (2%) alloys. The brittle fracture mode of the as-cast Zn-Ti alloys is consistent with its low elongation.

7 Reference List

- [1] V.L. Roger, A.S. Go, D.M. Lloyd-Jones, E.J. Benjamin, J.D. Berry, W.B. Borden, D.M. Bravata, S. Dai, E.S. Ford, C.S. Fox, H.J. Fullerton, C. Gillespie, S.M. Hailpern, J.A. Heit, V.J. Howard, B.M. Kissela, S.J. Kittner, D.T. Lackland, J.H. Lichtman, L.D. Lisabeth, D.M. Makuc, G.M. Marcus, A. Marelli, D.B. Matchar, C.S. Moy, D. Mozaffarian, M.E. Mussolino, G. Nichol, N.P. Paynter, E.Z. Soliman, P.D. Sorlie, N. Sotoodehnia, T.N. Turan, S.S. Virani, N.D. Wong, D. Woo, M.B. Turner, Heart Disease and Stroke Statistics—2012 Update, A Report From the American Heart Association 125(1) (2012) 2-220.
- [2] S.K. Bhatia, Biomaterials for Clinical Applications, Springer-Verlag New York, New York, NY, 2010.
- [3] R.A. Schatz, D.S. Baim, M. Leon, S.G. Ellis, S. Goldberg, J.W. Hirshfeld, M.W. Cleman, H.S. Cabin, C. Walker, J. Stagg, Clinical experience with the Palmaz-Schatz coronary stent. Initial results of a multicenter study, *Circulation* 83(1) (1991) 148-161.
- [4] T.R. Kucklick, The medical device R & D handbook, (2013).
- [5] J. Iqbal, J. Gunn, P.W. Serruys, Coronary stents: historical development, current status and future directions, *British Medical Bulletin* 106(1) (2013) 193-211.
- [6] A. Kastrati, D. Hall, A. Schömig, Long-term outcome after coronary stenting, *Current Controlled Trials in Cardiovascular Medicine* 1(1) (2000) 48-54.
- [7] S. Saito, New horizon of bioabsorbable stent, *Catheterization and Cardiovascular Interventions* 66(4) (2005) 595-596.
- [8] A. Colombo, E. Karvouni, Biodegradable Stents: "Fulfilling the Mission and Stepping Away", *Circulation* 102(4) (2000) 371-373.
- [9] P.K. Bowen, E.R. Shearier, S. Zhao, R.J. Guillory, F. Zhao, J. Goldman, J.W. Drelich, Biodegradable metals for cardiovascular stents: from clinical concerns to recent Zn - alloys, *Advanced healthcare materials* 5(10) (2016) 1121-1140.
- [10] M. Labinaz, J.P. Zidar, R.S. Stack, H.R. Phillips, Biodegradable Stents: The Future of Interventional Cardiology?, *Journal of Interventional Cardiology* 8(4) (1995) 395-405.
- [11] J.F. Tanguay, J.P. Zidar, H.R. Phillips, R.S. Stack, Current status of biodegradable stents, *Cardiology Clinics* 12(4) (1994) 699-713.
- [12] J. Kohn, J. Zeltinger, Degradable, drug-eluting stents: a new frontier for the treatment of coronary artery disease, *Expert Review of Medical Devices* 2(6) (2014) 667-671.
- [13] H. Hermawan, Biodegradable metals from concept to applications, Springer-Verlag Berlin Heidelberg, Berlin; New York, 2012.
- [14] M. Moravej, D. Mantovani, Biodegradable Metals for Cardiovascular Stent Application: Interests and New Opportunities, *International Journal of Molecular Sciences* 12(7) (2011) 4250-4270.

- [15] C. Di Mario, H.U.W. Griffiths, O. Goktekin, N. Peeters, J.A.N. Verbist, M. Bosiers, K. Deloose, B. Heublein, R. Rohde, V. Kasese, C. Ilsley, R. Erbel, Drug-Eluting Bioabsorbable Magnesium Stent, *Journal of Interventional Cardiology* 17(6) (2004) 391-395.
- [16] E.-O. MM, D. G, I. I, M. R, Update on In-stent Restenosis, *Current Interventional Cardiology Reports* 3(4) (2001) 9.
- [17] M. European Conference on Advanced, Processes, Euromat 2001 : 7th European conference on advanced materials and processes : Rimini, Italy, 10-14 June 2001, AIM, Milano, Italy, 2001.
- [18] G. Mani, M.D. Feldman, D. Patel, C.M. Agrawal, Coronary stents: A materials perspective, *Biomaterials* 28(9) (2007) 1689-1710.
- [19] M. Peuster, C. Hesse, T. Schloo, C. Fink, P. Beerbaum, C. von Schnakenburg, Long-term biocompatibility of a corrodible peripheral iron stent in the porcine descending aorta, *Biomaterials* 27(28) (2006) 4955-4962.
- [20] M. Peuster, P. Wohlsein, M. Brugmann, M. Ehlerding, K. Seidler, C. Fink, H. Brauer, A. Fischer, G. Hausdorf, A novel approach to temporary stenting: degradable cardiovascular stents produced from corrodible metal-results 6-18 months after implantation into New Zealand white rabbits, *Heart* 86 (2001) 563-569.
- [21] P.K. Bowen, J. Drelich, J. Goldman, Zinc exhibits ideal physiological corrosion behavior for bioabsorbable stents, *Advanced materials* 25(18) (2013) 2577-2582.
- [22] B. Henning, M. Toborek, C.J. McClain, Antiatherogenic properties of zinc: implications in endothelial cell metabolism, *Nutrition* 12(10) (1996) 711-717.
- [23] P.W. Serruys, M.J.B. Kutryk, A.T.L. Ong, Coronary-Artery Stents, *New England Journal of Medicine* 354(5) (2006) 483-495.
- [24] C.-C. Chu, H.P. Greisler, J.A. Von Fraunhofer, Wound closure biomaterials and devices, CRC Press, Boca Raton 1997.
- [25] P. Erne, M. Schier, T.J. Resink, The road to bioabsorbable stents: reaching clinical reality?, *Cardiovascular and Interventional Radiology* 29(1) (2006) 11-16.
- [26] M. Minerals, S. Materials, Magnesium technology 2011, John Wiley & Sons, New York, 2011.
- [27] G. Song, Control of biodegradation of biocompatible magnesium alloys, *Corrosion Science* 49(4) (2007) 1696-1701.
- [28] N.H. F. Witte, F. Feyerabend, C. Vogt, Magnesium (Mg) corrosion: a challenging concept for degradable implants, Woodhead, Philadelphia, PA, USA, 2011.
- [29] E. Frossard, M. Bucher, F. Mächler, A. Mozafar, R. Hurrell, Potential for increasing the content and bioavailability of Fe, Zn and Ca in plants for human nutrition, *Journal of the Science of Food and Agriculture* 80(7) (2000) 861-879.

- [30] M. Fontecave, J.L. Pierre, Iron: Metabolism, toxicity and therapy, *Biochimie* 75(9) (1993) 767-773.
- [31] D. Pierson, J. Edick, A. Tauscher, E. Pokorney, P. Bowen, J. Gelbaugh, J. Stinson, H. Getty, C.H. Lee, J. Drelich, J. Goldman, A simplified in vivo approach for evaluating the bioabsorbable behavior of candidate stent materials, *Journal of Biomedical Materials Research Part B: Applied Biomaterials* 100(1) (2012) 58-67.
- [32] H. Hermawan, A. Purnama, D. Dube, J. Couet, D. Mantovani, Fe–Mn alloys for metallic biodegradable stents: Degradation and cell viability studies, *Acta Biomaterialia* 6(5) (2010) 1852-1860.
- [33] H. Hermawan, D. Dubé, D. Mantovani, Degradable metallic biomaterials: Design and development of Fe-Mn alloys for stents, *Journal of Biomedical Materials Research Part A* 93(1) (2010) 1-11.
- [34] H. Hermawan, M. Moravej, D. Dubé, M. Fiset, D. Mantovani, Degradation Behaviour of Metallic Biomaterials for Degradable Stents, *Advanced Materials Research* 15-17 (2007) 113-118.
- [35] H. Hermawan, D. Dubé, D. Mantovani, Development of Degradable Fe-35Mn Alloy for Biomedical Application, *Advanced Materials Research* 15-17 (2007) 107-112.
- [36] M. Moravej, A. Purnama, M. Fiset, D. Mantovani, J. Couet, Electroformed pure iron as a new biomaterial for degradable stents: In vitro degradation and preliminary cell viability studies, *Acta Biomaterialia* 6(5) (2010) 1843-1851.
- [37] M. Moravej, F. Prima, M. Fiset, D. Mantovani, Electroformed iron as new biomaterial for degradable stents: Development process and structure-properties relationship, *Acta Biomaterialia* 6(5) (2010) 1726-1735.
- [38] B. Liu, Y.F. Zheng, Effects of alloying elements (Mn, Co, Al, W, Sn, B, C and S) on biodegradability and in vitro biocompatibility of pure iron, *Acta Biomaterialia* 7(3) (2011) 1407-1420.
- [39] Z. Li, X. Gu, S. Lou, Y. Zheng, The development of binary Mg-Ca alloys for use as biodegradable materials within bone, *Biomaterials* 29(10) (2008) 1329-1344.
- [40] L. Li, J. Gao, Y. Wang, Evaluation of cyto-toxicity and corrosion behavior of alkali-heat-treated magnesium in simulated body fluid, *Surface & Coatings Technology* 185(1) (2004) 92.
- [41] R. Bonan, A.W. Asgar, Biodegradable Stents - Where Are We In 2009?, *US Cardiology* 6(2) (2009) 81-84.
- [42] B. Heublein, R. Rohde, V. Kaese, M. Niemeyer, W. Hartung, A. Haverich, Biocorrosion of magnesium alloys: a new principle in cardiovascular implant technology?, *Heart* 89 (2003) 651-656.
- [43] B. Heublein, R. Rohde, M. Niemeyer, V. Kaese, W. Hartung, C. Rocken, Degradation of metallic alloys-A new principle in stent technology?, *Journal of the American College of Cardiology* 35 (2000) 14-15.

- [44] D. Schranz, P. Zartner, I. Michel-Behnke, H. Akintürk, Bioabsorbable metal stents for percutaneous treatment of critical recoarctation of the aorta in a newborn, *Catheterization and Cardiovascular Interventions* 67(5) (2006) 671-673.
- [45] J.A. Ormiston, P.W.S. Serruys, Bioabsorbable Coronary Stents, *Circulation Cardiovascular Interventions* 2(3) (2009) 255-260.
- [46] R. Waksman, R. Erbel, C. Di Mario, J. Bartunek, B. de Bruyne, F.R. Eberli, P. Erne, M. Haude, M. Horrigan, C. Ilesley, D. Böse, H. Bonnier, J. Koolen, T.F. Lüscher, N.J. Weissman, Early- and Long-Term Intravascular Ultrasound and Angiographic Findings After Bioabsorbable Magnesium Stent Implantation in Human Coronary Arteries, *JACC: Cardiovascular Interventions* 2(4) (2009) 312-320.
- [47] A.C. Hänzi, I. Gerber, M. Schinhammer, J.F. Löffler, P.J. Uggowitzer, On the in vitro and in vivo degradation performance and biological response of new biodegradable Mg-Y-Zn alloys, *Acta biomaterialia* 6(5) (2010) 1824-1833.
- [48] A.C. Hänzi, A.S. Sologubenko, P.J. Uggowitzer, Design Strategy for Microalloyed Ultra-Ductile Magnesium Alloys for Medical Applications, *Materials Science Forum* 618-619 (2009) 75-82.
- [49] A.C. Hanzi, P. Gunde, M. Schinhammer, P.J. Uggowitzer, On the biodegradation performance of an Mg-Y-RE alloy with various surface conditions in simulated body fluid, *Acta Biomaterialia* 5(1) (2009) 162-171.
- [50] K.M. Hambidge, N.F. Krebs, Zinc deficiency: a special challenge, *Journal of Nutrition* 137(4) (2007) 1101-1105.
- [51] P.J. Aggett, J.T. Harries, Current status of zinc in health and disease states, *Archives of Disease in Childhood* 54(12) (1979) 909-917.
- [52] M. Berger, Zinc reduces intimal hyperplasia in the rat carotid injury model, *Atherosclerosis* 175(2) (2004) 229-234.
- [53] J. Cheng, B. Liu, Y.H. Wu, Y.F. Zheng, Comparative in vitro Study on Pure Metals (Fe, Mn, Mg, Zn and W) as Biodegradable Metals, *Journal of Materials Science & Technology* 29(7) (2013) 619-627.
- [54] D. Vojtech, J. Kubasek, J. Serak, P. Novak, Mechanical and corrosion properties of newly developed biodegradable Zn-based alloys for bone fixation, *Acta Biomaterialia* 7(9) (2011) 3515-3522.
- [55] E. Mostaed, M. Sikora-Jasinska, A. Mostaed, S. Loffredo, A.G. Demir, B. Previtali, D. Mantovani, R. Beanland, M. Vedani, Novel Zn-based alloys for biodegradable stent applications: Design, development and in vitro degradation, *Journal of the Mechanical Behavior of Biomedical Materials* 60 (2016) 581-602.
- [56] C. Yao, S.L. Tay, T. Zhu, H. Shang, W. Gao, Effects of Mg content on microstructure and electrochemical properties of Zn-Al-Mg alloys, *Journal of Alloys and Compounds* 645 (2015) 131-136.

- [57] J. Kubásek, D. Vojtěch, E. Jablonská, I. Pospíšilová, J. Lipov, T. Ruml, Structure, mechanical characteristics and in vitro degradation, cytotoxicity, genotoxicity and mutagenicity of novel biodegradable Zn-Mg alloys, *Materials science & engineering. C, Materials for biological applications* 58 (2016) 24-35.
- [58] M. Avedesian, H. Baker, *ASM specialty handbook : magnesium and magnesium alloys*, ASM International, Materials Park, Ohio, 1999.
- [59] J.A. Helsen, H.J.r. Breme, *Metals as biomaterials*, Wiley, Chichester, 1998.
- [60] J.Z. Ilich, J.E. Kerstetter, Nutrition in bone health revisited: a story beyond calcium, *Journal of the American College of Nutrition* 19(6) (2000) 715-737.
- [61] H.F. Li, X.H. Xie, Y.F. Zheng, Y. Cong, F.Y. Zhou, K.J. Qiu, X. Wang, S.H. Chen, L. Huang, L. Tian, L. Qin, Development of biodegradable Zn-1X binary alloys with nutrient alloying elements Mg, Ca and Sr, *Scientific reports* 5 (2015).
- [62] H. Li, H. Yang, Y. Zheng, F. Zhou, K. Qiu, X. Wang, Design and characterizations of novel biodegradable ternary Zn-based alloys with IIA nutrient alloying elements Mg, Ca and Sr, *Materials & Design* 83 (2015) 95-102.
- [63] X. Liu, J. Sun, F. Zhou, Y. Yang, R. Chang, K. Qiu, Z. Pu, L. Li, Y. Zheng, Micro-alloying with Mn in Zn-Mg alloy for future biodegradable metals application, *Materials & Design* 94 (2016) 95-104.
- [64] X. Liu, J. Sun, K. Qiu, Y. Yang, Z. Pu, L. Li, Y. Zheng, Effects of alloying elements (Ca and Sr) on microstructure, mechanical property and in vitro corrosion behavior of biodegradable Zn-1.5Mg alloy, *Journal of Alloys and Compounds* 664 (2016) 444-452.
- [65] S. Zhao, C.T. McNamara, P.K. Bowen, N. Verhun, J.P. Braykovich, J.W. Drelich, J. Goldman, Structural Characteristics and In Vitro Biodegradation of a Novel Zn-Li Alloy Prepared by Induction Melting and Hot Rolling, *Metallurgical and Materials Transactions A* 48(3) (2017) 1204-1215.
- [66] P.K. Bowen, J.M. Seitz, J.P. Braykovich, S. Zhao, J.W. Drelich, R.J. Guillory, J. Goldman, Evaluation of wrought Zn-Al alloys (1, 3, and 5 wt % Al) through mechanical and in vivo testing for stent applications, *Journal of Biomedical Materials Research - Part B Applied Biomaterials* (2017).
- [67] J. Niu, Z. Tang, H. Huang, J. Pei, H. Zhang, G. Yuan, W. Ding, Research on a Zn-Cu alloy as a biodegradable material for potential vascular stents application, *Materials Science and Engineering: C* 69 (2016) 407-413.
- [68] X.K. Li, C.F. Yuan, J.L. Wang, Y.Q. Zhang, Z.Y. Zhang, Z. Guo, The treatment effect of porous titanium alloy rod on the early stage talar osteonecrosis of sheep, *PLoS ONE* 8(3) (2013).
- [69] M. Long, H.J. Rack, Titanium alloys in total joint replacement—a materials science perspective, *Biomaterials* 19(18) (1998) 1621-1639.

- [70] S.R. Paital, N.B. Dahotre, Calcium phosphate coatings for bio-implant applications: Materials, performance factors, and methodologies, *Materials Science and Engineering: R: Reports* 66(1-3) (2009) 1-70.
- [71] C. Aparicio, F. Javier Gil, C. Fonseca, M. Barbosa, J.A. Planell, Corrosion behaviour of commercially pure titanium shot blasted with different materials and sizes of shot particles for dental implant applications, *Biomaterials* 24(2) (2003) 263-273.
- [72] M. Niinomi, Recent metallic materials for biomedical applications, *Metallurgical and Materials Transactions A* 33 (2002) 477-486.
- [73] R. Noort, Titanium: The implant material of today, *Journal of Materials Science* 22(11) (1987) 3801-3811.
- [74] H.J.M. Bowen, *Environmental Chemistry : Volume 2*, (2007).
- [75] M. Institute of, Food, B. Nutrition, M. Institute of, M. Panel of, Dietary reference intakes for vitamin A, vitamin K, arsenic, boron, chromium, copper, iodine, iron, manganese, molybdenum, nickel, silicon, vanadium, and zinc : a report of the Panel on Micronutrients, National Academy Press, Washington, DC, 2002.
- [76] J.E. Bringas, *Handbook of comparative world steel standards*, ASTM, West Conshohocken, PA, 2004.
- [77] R. Lazarova, R.H. Petrov, V. Gaydarova, A. Davidkov, A. Alexeev, M. Manchev, V. Manolov, Microstructure and mechanical properties of P265GH cast steel after modification with TiCN particles, *Materials & Design* 32(5) (2011) 2734-2741.
- [78] A. Bedolla-Jacuinde, R. Correa, J.G. Quezada, C. Maldonado, Effect of titanium on the as-cast microstructure of a 16%chromium white iron, *Materials Science and Engineering: A* 398(1-2) (2005) 297-308.
- [79] S. Matsuo, T. Ando, N.J. Grant, Grain refinement and stabilization in spray-formed AISI 1020 steel, *Materials Science and Engineering: A* 288(1) (2000) 34-41.
- [80] Y. Tomita, K. Okabayashi, Effect of microstructure on strength and toughness of heat-treated low alloy structural steels, *Metallurgical Transactions A* 17(7) (1986) 1203-1209.
- [81] M. Jaradeh, T. Carlberg, Effect of titanium additions on the microstructure of DC-cast aluminium alloys, *Materials Science and Engineering: A* 413-414 (2005) 277-282.
- [82] N. Saheb, T. Laoui, A.R. Daud, M. Harun, S. Radiman, R. Yahaya, Influence of Ti addition on wear properties of Al–Si eutectic alloys, *Wear* 249(8) (2001) 656-662.
- [83] S. Li, H. Imai, H. Atsumi, K. Kondoh, A. Kojima, Y. Kosaka, K. Yamamoto, M. Takahashi, The effects of Ti and Sn alloying elements on precipitation strengthened Cu40Zn brass using powder metallurgy and hot extrusion, *Materials Science and Engineering: A* 535 (2012) 22-31.
- [84] G.L. Leone, H.W. Kerr, Grain structures and coupled growth in Zn-Ti alloys, *Journal of Crystal Growth* 32(1) (1976) 111-116.

- [85] G. Boczkal, Structure and properties of Zn-Ti_{0.2}-Cu_{0.15} single crystal containing eutectic precipitates, *Archives of Metallurgy and Materials* 58(4) (2013) 1019-1022.
- [86] M. Saillard, G. Develey, C. Becele, J.M. Moreau, D. Paccard, The Structure of ZnTi₁₆, *Acta Crystallographica Section B* 37B (1981) 224-226.
- [87] E.A. Anderson, E.J. Boyle, R. P.W, Rolled Zinc-titanium Alloys, *Transactions of the American Institute of Mining and Metallurgical Engineers* 156 (1944) 278-287.
- [88] G.R. Schulze, *Metallphysik*, Akademie-Verlag, Berlin, 1967.
- [89] Y. Prawoto, *Integration of mechanics into materials science research : a guide for material researchers in analytical, computational and experimental methods*, 2013.
- [90] D.R. Askeland, P.P. Fulay, D.K. Bhattacharya, *Essentials of materials science & engineering*, Cengage Learning, Stamford, CT, 2010.
- [91] J.W. Martin, *Micromechanisms in particle-hardened alloys*, Cambridge University Press, Cambridge, U.K., 1980.
- [92] A. International, *Standard Test Methods for Tension Testing of Metallic Materials*, West Conshohocken, PA, 2016.
- [93] M. Sikora-Jasinska, E. Mostaed, A. Mostaed, R. Beanland, D. Mantovani, M. Vedani, Fabrication, mechanical properties and in vitro degradation behavior of newly developed Zn Ag alloys for degradable implant applications, *Materials Science and Engineering: C* 77 (2017) 1170-1181.
- [94] J.A. Spittle, The effects of composition and cooling rate on the as-cast microstructures of Zn-Ti alloys, *Metallography* 5(5) (1972) 423-447.
- [95] G.F. Vander Voort, S.R. Lampman, B.R. Sanders, G.J. Anton, C. Polakowski, *ASM Handbook, Volume 9: Metallography and Microstructures. Vol. 9*, ASM International, Fort Lauderdale, 2004.
- [96] H. Gong, K. Wang, R. Strich, J.G. Zhou, In vitro biodegradation behavior, mechanical properties, and cytotoxicity of biodegradable Zn-Mg alloy, *Journal of Biomedical Materials Research Part B: Applied Biomaterials* 103(8) (2015) 1632-1640.
- [97] W.D. Callister, D.G. Rethwisch, *Materials Science and Engineering: An Introduction*, 2012.
- [98] M. Aliofkhazraei, *Handbook of mechanical nanostructuring*, 2015.

Appendix A. Copyright documentation



COPYRIGHT PERMISSION REQUEST

Please complete all contact information:

Name: Zhiyong Yin Title: Graduate Research Assistant
Company/Organization: Michigan Technological University
Address: 1400 Townsend Drive, M & M Building 423
City/State/Zip/Country: Houghton, MI 49931
Phone: 406-221-6824 Email: zhyin@mtu.edu

I am preparing an article/chapter for publication in the following formats (check as applicable):

Print Only Internet Only Print and Electronic Media

The information will be used for (check as applicable):

Journal article Conference presentation Internal company records
Dissertation Student course material Commercial publication*

Please complete the following:

The article/chapter title will be: Goals and Hypotheses

The publication title will be: MICROSTRUCTURAL EVOLUTION AND MECHANICAL PROPERTIES OF Zn-Ti ALLOYS FOR BIO

Publisher: Michigan Technological University

Planned date of publication: Fall 2017/Spring 2018

I hereby request permission for non-exclusive world rights for the above publication and all subsequent editions, revisions, and derivative works in English and foreign translations, in the formats indicated above from the following copyrighted content by ASM International:

Book ISBN: Copyright date: 1944
Book/Publication title: Trans. Am. Inst. Min. Metall. Pet. Eng.
Author name(s): Anderson E.A., Boyle E.J., and Ramsey P.W.
Article title: Rolled Zinc-titanium Alloys
Text page numbers:
Figure numbers (with page numbers):
Table numbers (with page numbers):

Signature: *Zhiyong Yin*

Date: 11/6/2017

FOR ASM INTERNATIONAL USE ONLY:

I (we) grant permission requested above. Please ensure that ASM International receives proper credit as publisher by citing the above ASM publication as a reference and including the following: Reprinted with permission of ASM International. All rights reserved. www.asminternational.org

ASM International Representative: Sue Sellers

Copyright © 2017 ASM International, Inc. All rights reserved. ASM International, Inc. is a registered trademark of ASM International, Inc.

Date: 11-10-2017

*For Commercial Publications, a copyright permission fee of \$50 per figure will be assessed. Exceptions can be made for reuse of content by its original authors.

ASM International, Permissions, 9639 Kinsman Road, Materials Park, Ohio 44073-0002
permissions@asminternational.org, Phone: 440-338-5151 x5465, Fax: 440-338-8542

SUBMIT

Figure A.1. Copyright permission for the Zn-Ti phase diagram from Figure 3.1a.